University of Alberta

Investigating the ^{197}Au-^{31}P Spin-Spin Coupling Interactions in Gold-Phosphine Halides using Solid-State Nuclear Magnetic Resonance, Spectral Simulations, and Quantum Chemistry Computations

by

Jerrod Ryan Dwan

A thesis submitted to the Faculty of Graduate Studies and Research

in partial fulfillment of the requirements for the degree of

Master of Science

Department of Chemistry

Spring 2011

Edmonton, Alberta

Abstract

Phosphorus-31 nuclear magnetic resonance spectroscopy with magic angle spinning was used to characterize ^{197}Au-^{31}P spin-spin coupling interactions in solid gold-phosphine halides and the spectra have been analyzed using perturbation theory. The ^{197}Au nucleus has a natural abundance of 100%, a spin of 3/2, and one of the smallest nuclear magnetic moments of all spin-active nuclei. Gold-197 has a very large nuclear quadrupole moment that leads to ^{197}Au nuclear quadrupolar coupling constants of approximately 1 GHz, and thus the Zeeman interaction for ^{197}Au is a perturbation on the quadrupolar interaction. The indirect spin-spin coupling constants, $^{1}J(^{197}\mathrm{Au},^{31}\mathrm{P})$, extracted from our experiments are compared with those calculated using quantum chemistry computations. The calculations show that the Fermi-contact mechanism is the most important spin-spin coupling mechanism. Anisotropy in the ^{197}Au-^{31}P spin-spin coupling was shown to arise from the spin-dipolar Fermi-contact cross-term, and that its magnitude is on the same order as $^{1}J(^{197}\mathrm{Au},^{31}\mathrm{P})_{\mathrm{iso}}$.

Table of Contents

List of Tables

List of Figures

List of Appendices

List of Symbols

α, β, γ – Euler angles

B_o – applied magnetic field strength

B_1 – radiofrequency field strength

C_Q – nuclear quadrupolar coupling constant

c – speed of light

D – direct dipolar coupling tensor

δ_{ii} – principal component of the chemical shift tensor

δ_{iso} – isotropic chemical shift

$\Delta\sigma$ – anisotropy of the chemical shift tensor

ΔJ – anisotropy of the indirect spin-spin coupling tensor

e – elementary charge

θ, φ – polar angles

γ_I –magnetogyric ratio for spin I

h – Planck's constant

$\hbar$ – reduced Planck's constant

$\hat{H}$ – Hamiltonian operator

η_σ – asymmetry of the chemical shift tensor

η_J – asymmetry o the indirect spin-spin coupling tensor

η_Q – asymmetry of the electric field gradient tensor

I – nuclear spin angular momentum operator

I – nuclear spin quantum number

J – indirect spin-spin coupling tensor

J_{iso} – indirect spin-spin coupling constant

J_{ii} – principal component of the indirect spin-spin coupling tensor

K – reduced indirect spin-spin coupling tensor

K – reduced indirect spin-spin coupling constant

κ – skew of the nuclear magnetic shielding or chemical shift tensor

m_e – electron mass

m_I – magnetic quantum number for spin I

μ_I – nuclear magnetic moment for spin I

μ_0 – vacuum permeability

μ_B – Bohr magneton

ν_L – Larmor frequency

ν_{rot} – rotor spinning frequency

Q – nuclear quadrupole moment

Ω – span of the nuclear magnetic shielding or chemical shift tensor

R_{DD} – direct dipolar coupling constant

R_{eff} – effective direct dipolar coupling constant

σ – nuclear magnetic shielding tensor

σ_{ii} – principal component of the nuclear magnetic shielding tensor

σ_{iso} – isotropic nuclear magnetic shielding constant

T – temperature

T_1 – nuclear spin-lattice relaxation time

T_1^{-1} – nuclear spin-lattice relaxation rate

T_2 – nuclear spin-spin relaxation time

T_2^{-1} – nuclear spin-spin relaxation rate

V – electric field gradient tensor

V_{ii} – principal component of the electric field gradient tensor

List of Abbreviations

ADF	Amsterdam Density Functional
aq	aqueous
CP	cross polarization
CSA	chemical shift anisotropy
CW	continuous wave
DFT	density functional theory
dppm$AuCl_2$	bis (dichlorogold(I)) bis(diphenylphosphino) methane
DPPEAuCl	dichloro bis(diphenylphosphino ethane) digold
DZ	double-ζ
EFG	electric field gradient
FID	free induction decay
GIAO	gauge independent atomic orbitals
HF	Hartree-Fock
HOMO	highest occupied molecular orbital
LUMO	lowest unoccupied molecular orbital
MAS	magic angle spinning
MAE	magic angle effect
N.A.	natural abundance
NMR	nuclear magnetic resonance
NQR	nuclear quadrupole resonance
NR	non-relativistic
o.d.	outside diameter
PAS	principal axis system
Ph	phenyl

$(PhO)_3PAuCl$	triphenylphosphite gold chloride
ppm	parts per million
QZ4P	quadruple-ζ quadruply polarized
RACP	ramped-amplitude cross polarization
rf	radiofrequency
ssbs	spinning sidebands
SO	scalar with spin-orbit relativistic
SR	scalar relativistic
tbutAuCl	chloro [1,1’-biphenyl-2-yl)di-tert-butylphosphine] gold(I)
tppAuCl	triphenylphosphine gold chloride
TPPM	two-pulse phase-modulated (decoupling)
TZ2P	triple-ζ doubly polarized
XRD	X-ray diffraction
ZORA	zeroth order regular approximation

Chapter 1:

Introduction and Outline

1.1 Introduction

Gold phosphine complexes have been well studied over the years; however, no one has fully probed the spin-spin coupling interactions that occur between gold and phosphorus nuclei in these complexes. This is mainly attributed to the large nuclear quadrupole moment of ^{197}Au (spin I = 3/2, 100 % natural abundance) and the resulting large ^{197}Au nuclear quadrupolar coupling constants, C_Q, values. [1,2] The large ^{197}Au C_Q values and small nuclear magnetic moment of ^{197}Au make direct observation of the ^{197}Au NMR spectra impossible at this time; however, information concerning ^{197}Au, ^{31}P spin-spin coupling can be obtained from high-resolution ^{31}P NMR spectra of solid samples.[3]

Since ^{197}Au has a spin quantum number of 3/2, one might expect ^{197}Au-^{31}P spin-pairs to yield 1:1:1:1 multiplets in the ^{31}P NMR spectra acquired with magic angle spinning.[3] Instead, one observes distorted doublets or broad featureless ^{31}P NMR lineshapes.[4] Treating the ^{197}Au Zeeman interaction[5] as a perturbation of the ^{197}Au nuclear quadrupolar interaction,[6,7] one can rationalize the doublets observed in the ^{31}P NMR spectra acquired with MAS. In some cases, broad featureless ^{31}P NMR spectra are observed and attributed to partial self-decoupling of the ^{197}Au nuclei because of rapid ^{197}Au nuclear spin-relaxation – also a consequence of its large nuclear quadrupole moment and effective quadrupolar relaxation.

The goal of this research is to study the interactions that ^{197}Au-^{31}P spin-pairs undergo in gold phosphine complexes using solid-state nuclear magnetic resonance (SS-NMR) spectroscopy. The problem with studying ^{197}Au directly is that it has very large nuclear quadrupolar coupling constants that one expects broad linewidths in the ^{197}Au SS-NMR spectra, thus making it impossible to extract any information from the spectra. Another problem with studying ^{197}Au SS-NMR spectra is the small magnetogyric ratio, γ, and hence magnetic moment for ^{197}Au which makes ^{197}Au an insensitive nucleus and makes observing any spin-spin coupling interactions involving ^{197}Au impossible to observe using direct observation SS-NMR methods.[8] Therefore, we shall investigate ^{197}Au-^{31}P spin-spin coupling interactions in gold-phosphine complexes by observing the phosphorus nucleus directly using ^{31}P NMR and determining how the gold nucleus affects the phosphorus' magnetic environment. In addition to the ^{31}P NMR spectra, Amsterdam-Density Functional (ADF) theory calculations will be carried out on the gold phosphine halides studied to be compared with results acquired experimentally. Experimental ^{31}P NMR spectra will be acquired using ^{31}P{^{1}H} cross-polarization and high-power ^{1}H decoupling techniques that will transfer the ^{1}H magnetization to the ^{31}P thus enhancing the signal. By obtaining high quality ^{31}P NMR spectra, it should be possible to learn something about the ^{197}Au spin-lattice relaxation times, and in favourable cases, determine the values of the ^{197}Au-^{31}P indirect spin-spin coupling constants. Once ^{31}P NMR spectra have been acquired, they will be simulated to determine the values of the ^{197}Au-^{31}P coupling constants and then compared with those determined from ADF

calculations, which were performed for some of the gold phosphine halides studied.

1.2 Thesis Outline

This thesis will cover the necessary background information to understand the science taking place in the experiments and the analysis of the experimental results. Chapter 2 will begin with a discussion of the spectroscopic technique, Nuclear Magnetic Resonance (NMR), which will include a brief history of the technique and ways of analysing the spectra. Then some information will follow on the types of spin-spin coupling interactions that take place between nuclei while they are in a magnetic field as well as how they affect what is observed in an NMR spectrum. A discussion of how to simplify the spectra observed in the solid state will then follow. Following this, some background information about the gold complexes that were studied in this research and a description of the methods used to determine some of the spectral parameters will be given.

In Chapter 3, the instruments and experiments that were used to determine the intramolecular NMR interactions occurring in the aforementioned gold complexes will be discussed. This will include a detailed list of spectrometers, parameters optimized and used, as well as any other methods used in the analysis. Chapter 3 will also outline other methods that have been used to characterize these compounds and explain how these methods have been successful at observing these gold phosphine complexes up to this point.

In Chapter 4, the results of the experiments and the analyses are presented while giving insights on what those results tell us about the complexes. In addition, the crystal structure parameters will be presented.

In Chapter 5, some general comments on the research performed as well as any conclusions drawn from the experiments will be given. Suggestions for future study of these complexes and related systems will also be given in the hopes of further characterizing these types of complexes.

Chapter 2:

Background Information

2.1 NMR

Nuclear Magnetic Resonance is a spectroscopic technique that differentiates nuclei based on their magnetic moment's interaction with the magnetic field.

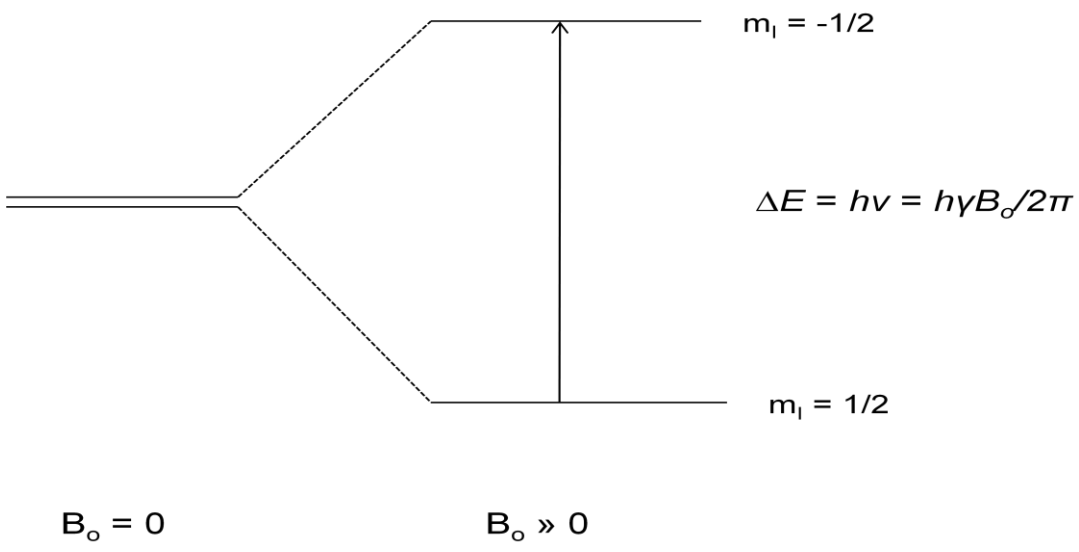

Fig. 2.1. Energy level diagram for a "bare" spin-1/2 nucleus (positive magnetogyric ratio, γ) in the absence and presence of an external magnetic field, B_0.

The interaction of the nuclear magnetic moment with an applied magnetic field is known as the Zeeman interaction. By applying a perturbing radiofrequency pulse at ν, this interaction is output in the form of a Free Induction Decay (FID) spectrum, the time domain spectrum. This FID is then Fourier transformed (FT) from the time domain to the frequency domain. The latter can then be interpreted

based on the position of the peak(s), their multiplicity (splitting), and their breadth.

How does all of this happen/work? The nucleus' magnetic moments are influenced directly by the magnetic field and, in the absence of any other field, some of these will align themselves with the magnetic field and others will not. For a spin I, there are 2I +1 Zeeman levels, e.g., for I = 3/2, there will be four Zeeman levels.[3] There will be slightly more magnetic moments aligned with the magnetic field than not, and it is this population difference that results in the signal observed in NMR. In a typical NMR experiment,[3] an external magnetic field in the radiofrequency (rf) range (i.e., a smaller magnetic field than that of the magnet) acts upon the nucleus in question for a period of time causing the nucleus' magnetic moment to be knocked from alignment with the external magnetic field. The rf signal is then measured as the magnetic moment realigns with the original magnetic field, thus yielding the FID. However, a typical NMR experiment deals with molecules and not just single nuclei so we must also take into account the effect that an individual nucleus' magnetic moment has on that of its neighbouring nuclei (see the section on coupling interactions). The motion of an electron about the nucleus can be considered as a small circuit that in turn generates a small magnetic field. This small magnetic field, which is generated by the electrons, then acts on that of neighbouring nuclei in addition to the external magnetic field. In this way, these nuclear magnetic fields slightly alter the overall magnetic field experienced by a nucleus' magnetic moment.

How do these fields affect the interaction between the nuclear magnetic moment and magnetic field? A magnetic field induces two kinds of electric current in a molecule: diamagnetic and paramagnetic.[9] The shielding constant is therefore given as the sum of the diamagnetic and paramagnetic contributions:

$$\sigma = \sigma_d + \sigma_p \qquad (2.1)$$

where σ is the shielding constant, σ_d is positive, and σ_p is generally negative. The diamagnetic term in *Equation 2.1* has a magnetization that is induced by an external field and acts in opposition to that field, however, the paramagnetic term's magnetization acts to augment the external field. Thus, a diamagnetic current gives rise to nuclear shielding while a paramagnetic current gives rise to nuclear deshielding.

Diamagnetic currents arise from electronic motion within atomic or molecular orbitals. The magnitude of the diamagnetic current is dependent on the electron density close to the nucleus and varies with the number of electrons. Meanwhile, paramagnetic currents arise from the electronic movement within molecules, like diamagnetic currents but in a different way. Where the diamagnetic current only deals with the ground electronic state of the molecule, paramagnetic currents deal in 'excited' states as well as ground states. Imagine a ground state (similar to a p_x orbital) that has two electrons with paired spins, and an unoccupied 'excited' state (similar to a p_y orbital). Applying an external magnetic field along the *z*-axis would overcome the energy gap between the ground and 'excited' state and allows the electrons to travel along the *xy* plane

instead of just being locked to the *x*-axis. This induced current then generates a magnetic field that augments the applied magnetic field and thus, deshields the nucleus at the centre of the electron density. The extent of this deshielding is dependent on the energy gap, $E_n - E_0$, between the two states[9,10] (see *Equation 2.2*); the smaller the gap, the greater the deshielding.

$$\sigma_{ii}^{p} = \frac{-\mu_0}{4\pi}\frac{e^2}{2m^2}\sum_{n>o}\frac{1}{E_n - E_0}\left[\left\langle 0\left|\sum_k \frac{l_{ki}}{r_k^3}\right|n\right\rangle\langle n|l_{ki}|0\rangle + \langle 0|\sum_k l_{ki}\,|n\rangle\left\langle n\left|\sum_k \frac{l_{ki}}{r_k^3}\right|0\right\rangle\right] \quad (2.2)$$

where μ_0 is the permeability of free space, *e* and *m* are the electron charge and rest mass, respectively, while <0| and <n| represent the ground and excited electronic states of the molecule with electronic energy E_0 and E_n, respectively. r_k is the position vector for electron *k* and l_{ki} is the angular momentum operator.

It was shown in 1949[11] that the frequency at which ^{14}N nucleus resonates is dependent on the chemical environment of that nucleus. It was later shown that this phenomenon in fact occurs for all nuclei; this phenomenon is referred to as nuclear magnetic shielding.

$$\nu = \frac{\gamma B_0}{2\pi}\,(1 - \sigma) \quad (2.3)$$

where σ is the shielding constant discussed earlier, γ is the magnetogyric ratio of the nucleus being observed, and B_o is the applied magnetic field. Chemical shifts

allow one to differentiate between chemical environments and this phenomenon makes NMR a powerful method of characterization. Typically, one measures chemical shifts rather than absolute shielding.[12] The chemical shift is measured according to *Equation 2.4*.

$$\delta = \frac{\nu_{sample} - \nu_{ref}}{\nu_{ref}} \approx \sigma_{ref} - \sigma_{sample} \qquad (2.4)$$

Due to the electronic nature of the shielding, chemical shift values will vary due to nuclear position in the molecule and therefore, any factors that affect the electrons about the nucleus also affect the chemical shift. From this, it can be shown that in a ^{1}H NMR spectrum, for example, protons belonging to differing functional groups or molecule types will have different shielding constants and therefore will give signals in different parts of the NMR spectrum.

In solution-state NMR, the differing chemical shifts of nuclei belonging to different functional groups allows the spectroscopist to identify the differing types of the nucleus being observed; this is what makes solution NMR such a powerful tool for structure determination. In addition, in the case of ^{1}H, one is able to determine the number of nuclei in a specific or similar chemical environment (i.e., for each type of nucleus) from the intensity of the signal observed. It may also be shown that the absorption (or resonance) frequencies of the nuclei are proportional to the magnitude of the applied magnetic field and, therefore, the chemical shift differences (in Hz) also increase with an increase in magnetic field as can be seen from *Equation 2.3*.

It is common to report chemical shift differences in parts per million (ppm) which is determined by taking the quotient of the measurement in Hertz (Hz) and the frequency of the spectrometer (ν) in MHz (see *Equation 2.4*). It is useful to convert chemical shift differences to dimensionless units, like ppm, as this helps when comparing values. The chemical shift difference is the negative of that for the magnetic shielding difference, therefore when there is a high frequency shift, it means that there is deshielding occurring.

In solid-state NMR, one is often dealing with powder samples in which all orientations of molecules in the applied magnetic field B_0 occur. Therefore, the spectrum results in a powder pattern that very rarely has the features observed in a solution spectrum. Due to the lack of averaging of the dipolar (and other) interactions that occurs for samples in solution, the lineshape is broadened. If one is to extract any information from a powder pattern, one must first attempt to determine the structure underneath the powder pattern. The reason the powder pattern appears is that in the solid-state, the spectrometer detects all orientations of the molecule and therefore gives a signal for each individual orientation. When these orientations are very similar, either the signals given for these orientations are in close proximity to one another or they are overlapping, causing the overall signal of these orientations to broaden. This range of chemical shift values is a result of shielding being orientation dependent and results in the powder pattern observed. When one also takes into account the interactions between nuclei that are in close proximity, then further broadening occurs that may result in the spectrum being almost featureless.

2.2 Spin-Spin Coupling Interaction Types

There are two kinds of spin-spin coupling interactions involved in NMR; dipolar (or direct) coupling and scalar (indirect) coupling. These two types of coupling interactions and their importance to NMR will be discussed below.

2.2.1 **Dipolar (direct) Coupling**

When a nucleus has a non-zero spin angular momentum, it also possesses a magnetic moment (*Equation 2.5*). These two factors are related through the magnetogyric ratio, which is unique to each isotope.

$$\boldsymbol{\mu}_N = \gamma_N \hbar \mathbf{I} \qquad (2.5)$$

where $\boldsymbol{\mu}_N$ is the nuclear magnetic moment, γ_N is the nuclear magnetogyric ratio, $\hbar$ is Planck's constant divided by 2π, and **I** is the spin angular momentum. As was discussed in the previous section, the electronic motion about the nucleus is effectively creating a magnetic field which the nuclear magnetic moment interacts with in addition to the applied magnetic field; however, this field is orders of magnitude smaller than fields that are typically used for NMR experiments.

In NMR experiments, one observes how these magnetic moments interact with not only the applied magnetic field, but with the magnetic moments of other nuclei as well.[13,14] The magnitude of the interaction (the direct dipolar coupling constant, R_{DD} *or* D) between the two nuclei is inversely proportional to the distance between the nuclei cubed (r^3). The dipolar coupling constant is given by

$$R_{DD} = \frac{\mu_0}{4\pi}\left(\frac{\gamma_I \gamma_S}{r^3}\right)\frac{\hbar}{2\pi} \quad (2.6)$$

where μ_0 is the permeability of the vacuum, γ_I and γ_S are the magnetogyric ratios of the coupled spins, *I* and *S*, and *r* is the distance between the coupled nuclei.

The direct dipolar tensor (*Equation 2.7*) shows that if r_{IS}, one of the principal components of the dipolar tensor, is aligned with the z-axis, the tensor is then diagonal.

$$\boldsymbol{D} = R_{\mathrm{DD}} \begin{bmatrix} 1 & 0 & 0 \\ 0 & 1 & 0 \\ 0 & 0 & -2 \end{bmatrix} \quad (2.7)$$

This is known as the principal axis system (PAS) of the dipolar tensor. It should also be noted that it is common to assume that the dipolar tensor is axially symmetric. The trace of the dipolar tensor is zero whether the tensor is axially symmetric or not, and it is because of this that the dipolar interaction does not affect the lineshape of NMR peaks in solution NMR. Due to molecular tumbling in solution an averaged signal is observed, and that average is zero. It is for the same reason that the dipolar interaction has no affect on the signals of spectra in the solid-state under magic angle spinning conditions, assuming that the spin rate is fast relative to the dipolar coupling constant (typically on the order of kHz) and that I and S are quantized by B_0 exclusively.

In order to take into account what is occurring in solid-state NMR, it is common to convert the Cartesian coordinates of the dipolar tensor to polar

coordinates. This is done by setting $x = r \sin\theta \cos\varphi$, $y = r \sin\theta \sin\varphi$, and $z = r \cos\theta$ and by expressing the spin operators of *x* and *y* as raising and lowering operators:

$$\hat{I}^{+} = \hat{I}_x + i\hat{I}_y \tag{2.8}$$

$$\hat{I}^{-} = \hat{I}_x - i\hat{I}_y \tag{2.9}$$

Spin functions are used to describe the nuclear spin states which are eigenfunctions of the Zeeman Hamiltonian and are often represented by $|I, m\rangle$. *I* represents the spin quantum number of the nucleus in question and *m* represents the z-component of the spin angular momentum and may take on values of $-I, -I+1, \ldots\ldots\ldots, I-1, I$. For example, if you have spin-½ nuclei, only two states exist: $|½, ½\rangle$, and $|½, -½\rangle$; these states are often referred to as $|\alpha\rangle$ and $|\beta\rangle$, respectively. Using polar coordinates, one can express the terms in the dipolar Hamiltonian, *Equation* 2.10, in terms of the 'dipolar alphabet.'

$$\mathbf{H}_{dd} = \gamma_1\gamma_2\hbar^2 \left\{\frac{\hat{I}_1 \cdot \hat{I}_2}{r^3} - \frac{3(\hat{I}_1 \cdot \boldsymbol{r})(\hat{I}_2 \cdot \boldsymbol{r})}{r^5}\right\} \frac{\mu_0}{4\pi} \tag{2.10}$$

All terms in the 'dipolar alphabet'[13] from *A* to *F* contain spin operators and spatial terms. In the presence of a strong magnetic field, only the *A* and *B* terms are relevant as the magnitudes of the other terms make them negligible in comparison.

$$A = -\hat{I}_{1z}\hat{I}_{2z}(3cos^2\theta - 1) \tag{2.11}$$

$$B = \frac{1}{4}\left[\hat{I}_1^{+}\hat{I}_2^{-} + \hat{I}_1^{-}\hat{I}_2^{+}\right](3cos^2\theta - 1) \tag{2.12}$$

where θ is the angle between the applied magnetic field and the axis of rotation. The *A* term does not affect the spin terms but the *B* term contains the 'flip-flop' operator which does affect the spin terms. The 'flip-flop' operator, in the case of a homonuclear two spin system, would change the |αβ> term to a |βα> term and vice versa. It is due to the $(3\cos^2\theta - 1)$ term in each of the dipolar alphabet terms that results in the dipolar coupling interaction being averaged to zero in solution. The $(3\cos^2\theta - 1)$ term shows the orientation dependence of the A and B terms. In the solid state what is called a powder pattern is observed, in the absence of anisotropic shielding or significant indirect coupling interactions, as all of the orientations of the dipolar vector with respect to the magnetic field are being observed (i.e., no averaging is occurring). The separation of the peaks observed in the powder pattern are dependent upon the angle, θ, and are equal to values of either $3R_{DD}$ (the shoulders of the spectrum, $\theta = 0^o$) or $3/2\ R_{DD}$ (the main peaks, $\theta = 90^o$) for spectra involving a homonuclear spin system if there is no chemical shift anisotropy (CSA). For unlike spin pairs, the separation between the main peaks is R_{DD} and they are centred about the frequency of the nucleus being observed. In the case of unlike spin pairs, the spectrum will consist of $2I + 1$ overlapping powder patterns, where *I* is the spin quantum number of the unobserved nucleus.

2.2.2 **Indirect (*J*) Coupling**

Indirect spin-spin coupling occurs over the course of two sequences. First, the spin state of a nucleus acts as a perturbation on the electrons that are moving about it. This perturbation can then be transferred to another nucleus through the electronic framework of the molecule to the second nucleus. This manner in

which the spin of one nucleus can affect that of another nucleus through the electrons in the molecule is known as the indirect spin-spin coupling interaction. The total spin-spin coupling constant, *J*, between a pair of nuclei is a combination of all the indirect coupling mechanisms that are taking place. The sign of the constant can be either positive or negative and the values of *J* are typically on the order of Hz, though values on the order of kHz are known. For example, the indirect coupling constant $^{1}J(^{199}\text{Hg}, ^{199}\text{Hg})$ for $Hg_3^{2+}$is approximately 140 kHz.[15] When the spin-spin coupling interaction helps in stabilizing the anti-parallel orientation of the nuclear spins, then *J* is positive in value. Knowing the value of J_{iso} is helpful in structure determination in solution state spectra as well as in the solid-state as specific types of functional groups or molecules have specific values of *J*.[16,17]

2.3 Quadrupolar Coupling

When a nucleus has a spin quantum number (*I*) greater than ½, it possesses a nuclear quadrupole moment, *Q*. This occurs due to the nucleus being non-spherical in shape and therefore possessing a non-spherical charge distribution; this is unlike the case of a spin-½ nucleus. There are two shapes which a quadrupolar nucleus can take, an oblate (discus shaped) or a prolate (cigar shaped), the main difference in these two shapes being the charge distribution. When a quadrupolar nucleus has a prolate shape, the sign of the quadrupole moment is positive, and the sign is negative for an oblate shape.[3] In NMR, the

nucleus' quadrupole moment interacts with the electric field gradient (EFG)[18,19] which may occur at the nucleus. A Hamiltonian[3] that incorporates the EFG tensor and the quadrupole moment may represent this quadrupolar interaction, as can be seen below.

$$h^{-1}H_Q = \frac{C_Q\,(3\hat{\mathbf{I}}_z^2 - \hat{\mathbf{I}}^2)}{4I\,(2I-1)} \qquad (2.13)$$

where $\hat{\mathbf{I}}^2|\mathrm{I}, \mathrm{m_I}\rangle = I(I+1)|\mathrm{I}, \mathrm{m_I}\rangle$ and $\hat{\mathbf{I}}_z|\mathrm{I}, \mathrm{m_I}\rangle = m_I|\mathrm{I}, \mathrm{m_I}\rangle$.

The EFG tensor in this case is symmetric and traceless. There are two parameters that are most often used to describe the EFG tensor: the largest component of the tensor (V_{zz} *or* eq_{zz}) and the asymmetry parameter (η_Q). (*Equation* 2.14)

$$\eta_Q = \frac{(q_{xx} - q_{yy})}{q_{zz}} \qquad (2.14)$$

The axes are chosen such that $|q_{zz}| \geq |q_{yy}| \geq |q_{xx}|$ so that $0 \leq \eta_Q \leq 1$ where $q_{zz} + q_{yy} + q_{xx} = 0$ (see Fig. 2.2).

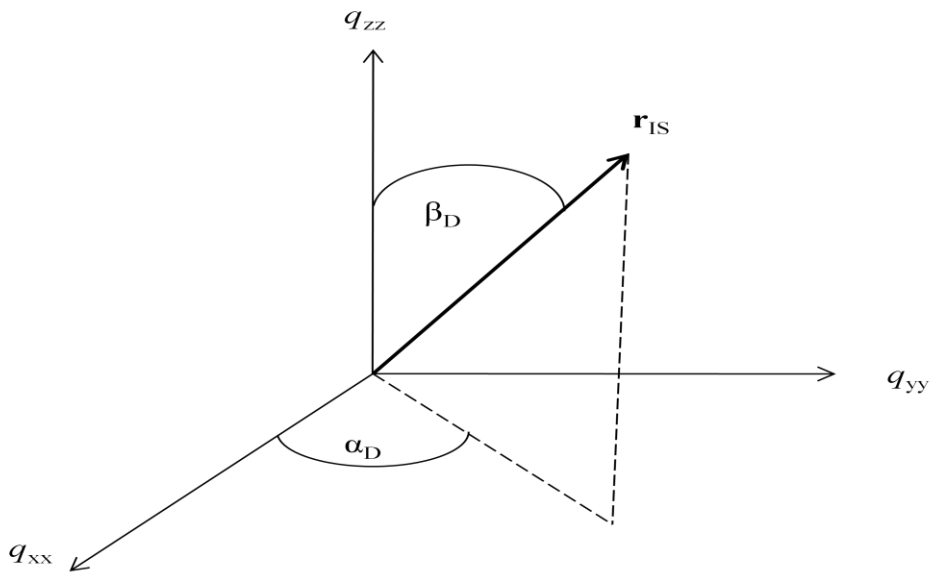

Fig. 2.2 Relative orientation of the dipolar vector, $\mathbf{r}_{IS}$, to the EFG tensor, where β_D is the angle between the largest component of the EFG tensor and the bond axis and α_D is the angle between the projection of the bond axis on the q_{xx}-q_{yy} plane and the smallest component of the EFG tensor.

The quadrupolar coupling constant, C_Q, is the product of the largest component of the EFG tensor and the nuclear quadrupole moment of the nucleus as can be seen in *Equation 2.15*:

$$C_Q = \frac{e^2 Q q_{zz}}{h} \qquad (2.15)$$

where e is the charge of an electron, Q is the nuclear quadrupole moment, eq_{zz} is the largest component of the electric field gradient tensor, and h is Planck's constant.

In NMR experiments involving quadrupolar nuclei, the nuclear quadrupolar coupling constant is generally much smaller than the Zeeman interaction (high field approximation); however, when there is little difference between the two, the energy levels of the quadrupolar nucleus are affected by both

the EFG and the applied magnetic field.[20,21,22] For the experiments conducted for this research, however, the quadrupolar interaction is several orders of magnitude larger than the Zeeman interaction. This would indicate that the energy levels of the quadrupolar nucleus are affected mainly by the EFG, and the Zeeman interaction is considered to act as a perturbation on the EFG.[7,23,24] If you have a situation where there is no applied magnetic field ($B_o = 0$) and a large C_Q is present then one will observe a Nuclear Quadrupole Resonance (NQR)[25] spectrum. While if there is a large applied magnetic field but no C_Q, then the spectrum acquired is similar to what is expected for a spin-½ nucleus.

When a powder is studied via NMR, a powder pattern is produced in the spin-½ NMR MAS spectrum, which consists of overlapping doublets (in the case of a spin-½ nucleus coupling to a spin-3/2 nucleus) when the C_Q value is much larger than that of the Zeeman interaction.[4,7] The peaks from the doublet will be due to the $m_I = ½ \rightarrow m_I = -½$ transition. The other transitions are less readily observed due to the broadening effect occurring as a result of their orientation dependence. In solution NMR, these effects are averaged due to molecular tumbling in a similar manner as it averages the dipolar contribution to spectra and only a single peak is observed. The averaging would not be enough to give sharp peaks as is usually expected in solution state NMR, however, with widths up to tens of kHz in some cases. These peaks can be affected by the EFG, and the EFG effect on linewidths is determined based on the local geometry about the nucleus. For example, a highly symmetric geometry (tetrahedral, octahedral, spherical,

etc.) in which the nucleus being studied is at the centre of symmetry will result in the EFG being equal to zero, i.e., there is no field gradient present.

2.4 Magic Angle Spinning

Magic Angle Spinning (MAS) is a technique that was developed as a possible solution to the broad lineshapes in spectra of powder samples observed by Solid-State NMR. The technique places the sample into a probe in such a way that it is at the magic angle relative to the direction of the magnetic field. The magic angle was calculated to be 54.74^{o} by setting the value $(3\cos^2\beta - 1)/2$ from the dipolar alphabet terms to zero[3] and then solving for β, where β is the angle between B_0 and the rotation axis. MAS is usually not applied in the case of solution state NMR as in a solution there is molecular tumbling going on which averages the interactions to their isotropic values. Thus, only an averaged signal is observed. This averaged signal makes for easier interpretation of spectra; however, it usually removes any dipolar coupling, CSA, and, in the case of solution spectra, EFG information.

As was discussed earlier in the section on dipolar coupling, all relevant terms in the 'dipolar alphabet',[13] and some of the terms in the quadrupolar Hamiltonian,[3] depend on a $(3\cos^2\theta - 1)$ term. If a solid sample is placed at an angle of 54.74^{0} relative to the applied magnetic field and spun sufficiently fast, then this will remove the effects due to dipolar interactions; however, it is not possible to average the quadrupolar coupling effects to zero, regardless of the spinning frequency. The objective of applying magic angle spinning is usually to

get sharp, solution-like spectra. The rate of spinning must be much greater than the interaction that is to be averaged, however, if the rate of spinning is equal to or less than the magnitude of the anisotropic interaction, spinning sidebands (ssb) will appear in the spectrum on either side of the isotropic peak, at intervals that are separated by the spinning frequency. These spinning sidebands can be used to determine some of the principal components in the chemical shift tensor[26,27] based on their intensities and positions if the spinning sidebands result only from anisotropic magnetic shielding. From this, one can infer that conducting MAS NMR experiments at slower rates could be used to get information about the anisotropic magnetic shielding interaction but still give spectra that are closer to solution-like spectra than what would be produced from a static NMR experiment.

2.5 Cross–Polarization Method

Cross polarization (CP) is a technique that enhances the signal of a less sensitive nucleus bonded to or close enough (for a significant dipolar coupling constant) to a spin-½ nucleus.[3,28,29] It does this by transferring the spin polarization of the sensitive nucleus to the less abundant nucleus assuming that the two nuclei are direct dipolar coupled. Why is this technique necessary? The reason that insensitive nuclei are more difficult to observe using NMR is that these insensitive nuclei tend to have quite long relaxation times (the time it takes for the spin angular momentum to return to alignment with the magnetic field after being offset by a radiofrequency field). Therefore, a typical NMR

experiment would produce very weak signals, as fewer scans would be acquired due to the long delays that would be required. However, by employing cross-polarization, the signal can be enhanced by using the relaxation time of the sensitive nucleus in place of that of the insensitive nucleus, thus enhancing the signal-to-noise of the resultant spectrum. The sensitive nucleus loses only a small amount of its spin polarization during this transfer to the insensitive nucleus, even if this means a large increase in the insensitive nucleus' spin polarization.

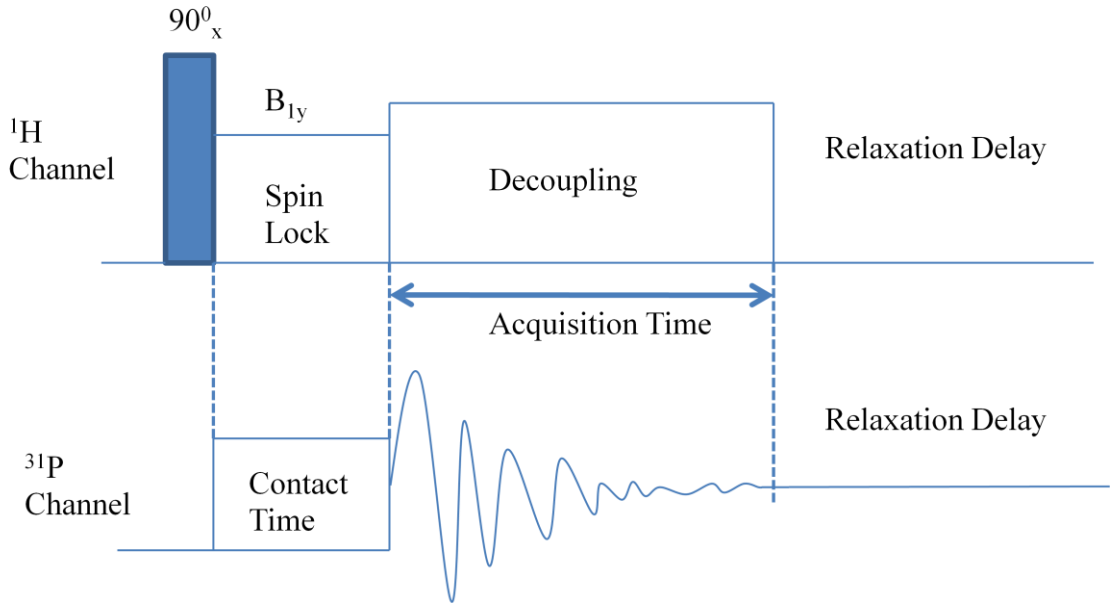

Fig. 2.3. Pulse sequence of cross-polarization from ^1H to ^{31}P where the 90^0 pulse is on the order of μs, the contact time is usually a few ms, the acquisition time is on the order of 100 ms, and the relaxation delay is on the order of seconds. (times are not to scale)

The most common form of CP experiment is known as Hartmann-Hahn CP, which results in the radiofrequency fields of the sensitive and insensitive nuclei to be matched so that they are equivalent; this is known as the Hartmann-Hahn matching condition (*Equation 2.16*).[30]

$$\gamma_I B_{1,I} = \gamma_S B_{1,S} \quad (2.16)$$

The signal enhancement produced can be as great as a factor of γ_I/γ_S and is dependent upon the strength of the dipolar coupling, i.e., the stronger the dipolar coupling the greater the signal enhancement. Spin polarization transfer between the two nuclei occurs during the time that both nuclei are being pulsed (contact time). Due to the dependence of the Hartmann-Hahn match condition on spinning rate and the resulting need to re-optimize field strengths when changing spinning rates, one should modify the typical CP pulse sequence in such a way that the field strength increases linearly (ramped-amplitude CP) to reduce this problem. This RACP[31] gives a wide range of Hartmann-Hahn match conditions that eliminates the requirement of re-optimizing the rf field strengths when changing spinning frequencies (*Fig.* 2.4).

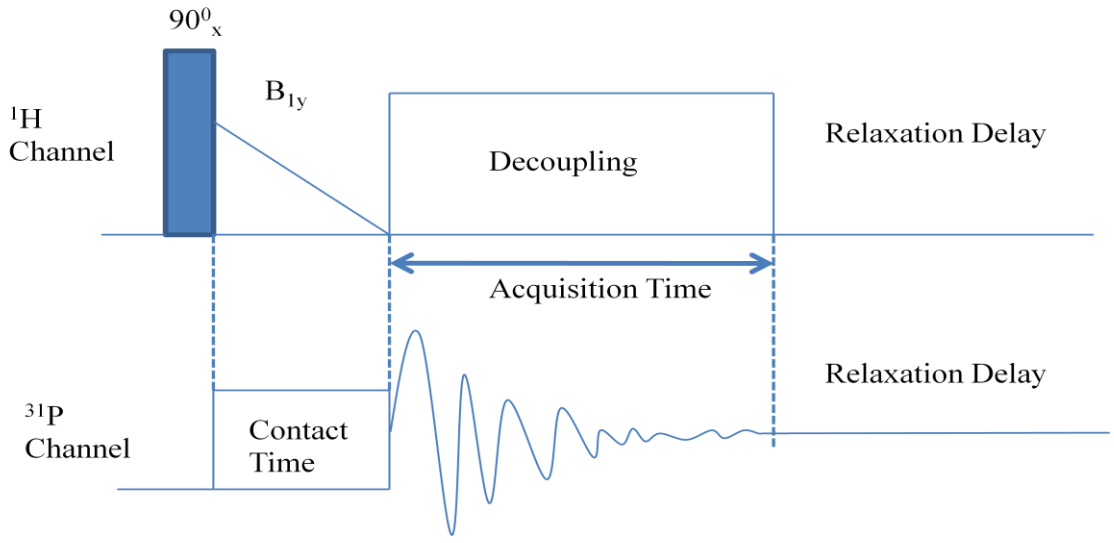

Fig. 2.4. Pulse sequence of RACP experiment from ^{1}H to ^{31}P where the 90^0 pulse is on the order of μs, the contact time is usually a few ms, the acquisition time is on the order of 100 ms, and the relaxation delay is on the order of seconds. (times are not to scale)

2.6 Perturbation Theory – Observing NMR Spectra of Spin-1/2 Nuclei adjacent to Quadrupolar Nuclei

In the case of spin-pairs where one spin is I = ½ and the other spin is quadrupolar, first-order perturbation theory is usually applied when the Zeeman interaction is much greater than the quadrupolar interaction; however, it has been shown that first-order perturbation theory can also be applied in the opposite scenario[18, 21-23] (i.e., the quadrupolar interaction is much greater than the Zeeman interaction). Here, first-order perturbation theory is applied where C_Q is much greater than ν_S (the Zeeman frequency of the quadrupolar nucleus) and the Zeeman interaction can be viewed as a perturbation on the quadrupolar interaction.

As shown below (*Fig.* 2.5), in these cases a doublet is observed in the ^{31}P MAS NMR spectrum when you have a spin-1/2 nucleus coupling to a spin-3/2 nucleus. The doublet is symmetric and insensitive to the sign of the quadrupolar coupling constant. This splitting is not inversely proportional to the field strength of the spectrometer. Due to the change from the usual first-order perturbation theory (i.e., Zeeman > Quadrupolar), the splitting that is observed is larger than what would be predicted from the first order theory for the high field approximation.

A method involving the ratio between the quadrupolar coupling constant and the Zeeman frequency has been developed[21] that allows one to predict the lineshapes of spectra where dipolar and indirect coupling between a spin-½

nucleus and a quadrupolar nucleus is taken into account. The only exception to this method is when $(C_Q/\nu_S) = 4$; in this case, the resulting spectrum is a triplet and the only way to determine the individual orientations of the transitions making up the central peak is by calculating the complete Zeeman-Quadrupolar Hamiltonian.[22] For values of $(C_Q/\nu_S) = 3$ or less, a quartet or disorted quartet is observed and for values of 5 or higher, a doublet is observed. In the case of the experiments for this research, the value for (C_Q/ν_S) is on the order of 100 or more and therefore a doublet would be expected due to some peaks overlapping with one another in accordance with the observed trend from the figure shown (*Figure* 2.5). First-order perturbation theory shows that the splitting observed in these spectra is roughly proportional to (DC_Q/ν_S). It should be noted that if the sign of the quadrupolar coupling constant is reversed then the line positions and the signs of the coefficients for the terms will be reversed as well. If one uses a known value for the quadrupolar coupling constant, one can use first-order perturbation theory to predict the value of J and its sign provided the sign of the quadrupolar coupling constant is known.

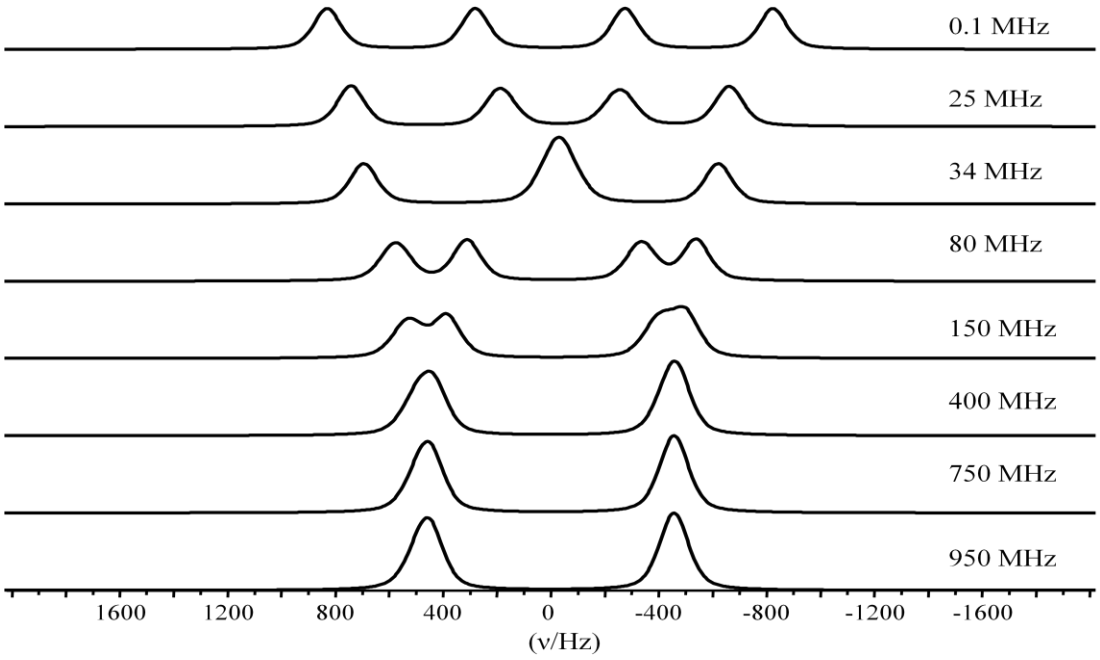

Fig. 2.5, ^{31}P NMR spectra calculated using WSOLIDS with typical ^{197}Au-^{31}P spin-pairs at B_0 = 11.75 T ($\nu(^{31}P)$ = 202.5 MHz, $\nu(^{197}Au)$ = 8.65 MHz) with varying C_Q values (seen at the right-hand side of the figure). Values of ^1J (^{197}Au, ^{31}P) = 550 Hz, R_{DD} = 76.0 Hz, ΔJ = 0, $\alpha = 0^0$, $\beta = 0^0$, and $\eta_Q = 0$ were used for these simulations. A 50% Gaussian: Lorentzian line broadening was used, with a broadening of 125 Hz for each type.

2.7 Gold Phosphine Complexes

Gold phosphine halides have been studied extensively in the past;[32,33,34] however, few of these studies have been conducted on these complexes using ^{31}P NMR in the solid state. There are a few reasons for why it is so difficult to extract coupling information from ^{31}P NMR spectra of gold phosphine halides. The first reason is that due to the very large quadrupolar coupling constant (C_Q) of ^{197}Au, a significant amount of line broadening occurs which may remove the hyperfine structure that is required to extract indirect coupling constant information from ^{31}P NMR spectra. Another reason is that ^{197}Au often has a very short relaxation time,

which makes it very difficult to observe using direct methods of NMR (i.e., ^{197}Au NMR), and this may result in further line broadening. Gold phosphine halides have been successfully studied employing other methods of spectroscopy, such as Mössbauer spectroscopy.[31,32] Studying these complexes using solid-state NMR while observing ^{197}Au directly, however, would seem to be an exercise in futility (for the time being); therefore, one should attempt to study the ^{197}Au nucleus indirectly.

One method to study gold phosphine halides is to analyze ^{31}P NMR spectra obtained in the solid-state to observe how they are affected by ^{197}Au. As was discussed in an earlier section, due to the large nature of C_Q(^{197}Au) (on the order of 1 GHz[2]), one would expect a doublet when observing the ^{31}P CP MAS spectrum of these gold phosphine halides. This is contrary to what is expected from a typical spectrum involving a spin-½ nucleus coupling to a spin-3/2 nucleus as a quartet is expected (*Fig. 2.3*). As was mentioned earlier, due to the C_Q being much greater in magnitude than the Zeeman interaction, the quadrupolar interaction is the governing factor in the spectrum so one would conclude that there is still a quartet in the structure of the spectrum. However, some of the signals are overlapping because of broadening due to the quadrupolar coupling interaction.

2.8 ADF Calculations

Amsterdam Density Functional (ADF)[35] theory is based on the Kohn-Sham approach to Density Functional Theory (DFT). ADF was a joint project

between theoretical chemistry groups from the Vrjie Universiteit in Amsterdam and the University of Calgary. The advantage ADF has over standard DFT is that ADF can be used to calculate properties of large molecules, including those that contain heavy metals. Some of the types of properties that can be calculated using ADF are those important in molecular spectroscopy, crystallography, pharmacochemistry, and organic and inorganic chemistry. ADF uses Slater-type basis functions and has many varieties of basis functions for each atom. It also takes advantage of molecular symmetry groups and linear scaling techniques to speed up calculations for larger molecules. ADF has many types of functionals available to it, such as local density approximation (LDA), generalized-gradient approximation (GGA), hybrid functionals, and meta-GGA functionals.

ADF was used for the purposes of this research to calculate the indirect coupling constant (^{1}J (^{197}Au, ^{31}P)) of each gold phosphine halide so that the value given by the calculations could be compared with those extracted from the NMR spectra of each gold phosphine halide. Several basis sets were tested to determine how well they were able to calculate the largest component of the EFG tensor for some simple gold-containing molecules and to compare those values with those given in the literature to determine an appropriate basis set and functional to use on the gold phosphine halide complexes studied by NMR.

Chapter 3:

Experiment (listing spectrometers with details, as well as calculations)

3.1 Chemagnetics CMX Infinity 200 NMR Spectrometer, 4.70*T*

^{31}P cross-polarization (CP), magic angle spinning (MAS), NMR data were obtained at ambient temperatures using a Chemagnetics CMX-200 spectrometer operating at a ^{31}P frequency of 81.02 MHz. Conventional RAMP cross-polarization, TPPM ^{1}H decoupling, and magic angle spinning techniques were employed using a 4 mm outer diameter (o.d.) rotor and spun at MAS frequencies of up to and including 15 kHz. Recycle delays of 240 seconds for triphenylphosphine gold (I) chloride, 210 seconds for bis (chlorogold (I)) bis (diphenylphosphino) methane, and 10 seconds for chloro [1,1'-biphenyl-2-yl) di-tert-butyl phosphine] gold (I) were used. A Hartmann-Hahn contact time of 3 ms and a ^{1}H $\pi/2$ pulse length of 4 μs were used for all spectra. All ^{31}P chemical shifts were referenced to 85% H_3PO_4 (*aq*) by setting the peak due to solid ammonium dihydrogen phosphate (ADP) to 0.81 ppm.[36]

3.2 Bruker Avance 300 NMR Spectrometer, 7.05 *T*

^{31}P CP MAS NMR data were obtained at ambient temperatures using a Bruker Avance 300 MHz WB-300 spectrometer operating at a ^{31}P frequency of 121.60 MHz. Conventional RAMP CP, TPPM ^{1}H decoupling, and MAS techniques were employed using a Bruker 4 mm rotor in which MAS frequencies of 5 kHz were achieved. Recycle delays of 600 seconds were used for tppAuCl

and $((dppm)AuCl)_2$ and of 10 seconds were used for (tbut)PAuCl. A Hartmann-Hahn contact time of 1 ms and a ^1H $\pi/2$ pulse length of 4 μs were used for all spectra with the exception of (tbut)PAuCl, in which case a contact time of 4 ms was used. All ^{31}P chemical shifts were referenced to 85% H_3PO_4 (*aq*) by setting the peak due to solid ammonium dihydrogen phosphate (ADP) to 0.81 ppm.[36]

3.3 Bruker Avance 500 NMR Spectrometer, 11.75 *T*

^{31}P CP MAS NMR data were collected at ambient temperatures using a Bruker Avance 500 MHz WB-500 spectrometer operating at a ^{31}P frequency of 202.53 MHz. Conventional RAMP CP, TPPM ^1H decoupling, and MAS techniques were employed using a Bruker 4 mm rotor in which MAS frequencies of up to and including 8 kHz were achieved. Recycle delays of 600 seconds for tppAuCl and $((dppm)AuCl)_2$ and 10 seconds for (tbut)PAuCl were used. A Hartmann-Hahn contact time of 5 ms and a ^1H $\pi/2$ pulse length of 4 μs were used for all spectra with the exception of $((dppm)AuCl)_2$, in which case a contact time of 2 ms was used. All ^{31}P chemical shifts were referenced to 85% H_3PO_4 (*aq*) by setting the peak due to solid ammonium dihydrogen phosphate (ADP) to 0.81 ppm.[36]

3.4 Bruker Avance 500 NMR Spectrometer (11.75 *T*) Variable Temperature Experiments

^{31}P MAS NMR data was obtained at variable temperature using a Bruker Avance 500 MHz WB-500 spectrometer operating at a ^{31}P frequency of 202.53 MHz. Conventional RAMP CP, TPPM ^1H decoupling, and MAS techniques were

employed using a Bruker 4 mm rotor in which MAS frequencies of 8 kHz were achieved. Recycle delays of 15 seconds were used for dichloro bis[(diphenylphosphino) ethane] digold. A Hartmann-Hahn contact time of 1 ms and a ^{1}H $\pi/2$ pulse length of 4 μs was used. All ^{31}P chemical shifts were referenced to 85% H_3PO_4 (*aq*) by setting the peak due to solid ammonium dihydrogen phosphate (ADP) to 0.81 ppm.[36]

3.5 Varian VNMRS 600 NMR Spectrometer, 14.09 *T*

^{31}P MAS NMR data was obtained at ambient temperature using a Varian 600 MHz narrow bore spectrometer operating at a ^{31}P frequency of 242.86 MHz. Conventional RAMP CP, TPPM ^{1}H decoupling, and MAS techniques were employed using a Varian 3.2 mm probe in which MAS frequencies of up to 11 kHz were achieved. Recycle delays of 300 seconds were used for triphenylphosphite gold chloride. A Hartmann-Hahn contact time of 1 ms and a ^{1}H $\pi/2$ pulse length of 2.25 μs was used. All ^{31}P chemical shifts were referenced to 85% H_3PO_4 (*aq*) by setting the peak due to solid ammonium dihydrogen phosphate (ADP) to 0.81 ppm.[36]

^{31}P NMR spectra of stationary samples were obtained at ambient temperature using a Varian 600 MHz narrow bore spectrometer operating at a ^{31}P frequency of 242.86 MHz. Conventional RAMP CP and TPPM ^{1}H decoupling techniques were employed using a Varian 3.2 mm probe. Recycle delays of 300 seconds were used for triphenylphosphite gold chloride. A ^{1}H $\pi/2$ pulse length of 2.25 μs was used. All ^{31}P chemical shifts were referenced to 85% H_3PO_4 (*aq*) by

setting the peak due to solid ammonium dihydrogen phosphate (ADP) to 0.81 ppm.[36]

3.6 Chemicals and Calculations

All chemicals used for the purposes of this research were purchased through Aldrich and all NMR experiments were conducted accordingly on those chemicals. With the exception of triphenylphosphite gold(I) chloride which was a purple powder, all the chemicals consisted of a white powder with a yellowish hue. For ADF calculations, P-Au-Cl bond angles of 180^0 were used with Au-P bond lengths of 2.3 Å and Au-Cl bond lengths of 2.29 Å. Data from the crystal structures for the compounds studied were entered into a structure program, such as GaussView or ChemCraft, and the resulting coordinates given by that program were used in the input file.

Chapter 4:

Results and Discussion

Table 4.1. ^{31}P NMR data for gold-phosphine complexes studied. δ_{iso} values at the magnetic field strengths used are in ppm and $^{1}J(^{197}Au, ^{31}P)$ values are in Hz.

Complex	4.70 T	7.05 T	11.75 T	14.09 T	^{1}J (^{197}Au, ^{31}P)/Hz
tppAuCl	30.1	30.3	30.3	--	550
tbutAuCl	61	61	61	--	520
dppm$AuCl_2$	28	28	28	--	630
DPPEAuCl	--	--	31	--	420
$(PhO)_3$PAuCl	--	--	--	11	--

4.1 Triphenylphosphine Gold (I) Chloride (tppAuCl)

Triphenylphosphine gold (I) chloride (*Fig.* 4.1) has been studied using ^{31}P CP MAS NMR spectroscopy in the solid-state at three fields: 4.70, 7.05, and 11.75 *T*. The spectra at each of these fields can be seen below.

Fig. 4.1. Crystal structure[37] for tppAuCl.

In the spectra produced at each field, a symmetric doublet is observed at about 30.3 ppm. This doublet is made up of two sets of overlapping pairs of powder patterns as illustrated in the figures below (*Figs.* 4.2, 4.3, and 4.4, respectively). Due to the long pulse delays required to produce high quality spectra, all NMR experiments on tppAuCl were allowed to acquire for anywhere from 2 days to up to a week. The splitting at all three fields was found to be on about 1 kHz indicating that the splitting is independent of field. From this, one would surmise that despite a further increase in the magnetic field strength of the spectrometer, it is not currently possible to observe the quartet that is expected when a spin-½ nucleus couples to a spin-3/2 nucleus. The reason for this is that due to the quadrupolar coupling constant being so much larger than the Zeeman frequency, the spectrometers are not able to resolve more than two of the signals. At these fields, the other two signals are still overlapping those two signals. From these spectra, the indirect coupling constant for ^{197}Au and ^{31}P (^{1}J (^{197}Au, ^{31}P)) was determined to be about 550 Hz, using the approximation that the splitting of the doublet is equal to 1.65 times the indirect coupling constant.[38] This value for ^{1}J (^{197}Au, ^{31}P) was later confirmed through simulations of the spectra using the WSOLIDS[39] simulation program. The previous value for ^{1}J (^{197}Au, ^{31}P) from the literature being 520 Hz as was reported by Bowmaker *et al.*,[38] so it can be seen that the agreement between the two values is acceptable.

For the simulation with WSOLIDS, a quadrupolar coupling constant of 940 MHz was used as was reported in the literature,[2] a dipolar coupling constant of 76 Hz was calculated using the bond length of the ^{197}Au and ^{31}P bond (2.23

Å),[37] and a line broadening of 390 Hz was used. Euler angles of $\alpha = \beta = 0^0$ were also used. With β being equal to 0^0, this implies that the largest component of the EFG tensor is along the $^{197}Au - {}^{31}P$ bond axis. The asymmetry parameter, η_Q, was set to a value of 0, indicating an axially symmetric EFG tensor. ADF calculations on tppAuCl yielded a C_Q value of 850 MHz and a η_Q value of 0.02, so the approximations for the simulations agree well with what is given in the ADF calculations. From X-ray studies,[37] the crystals are orthorhombic, space group $P2_12_12_1$ with four tppAuCl molecules occurring in the unit cell. There is D_2 symmetry and no three-fold rotation axis.

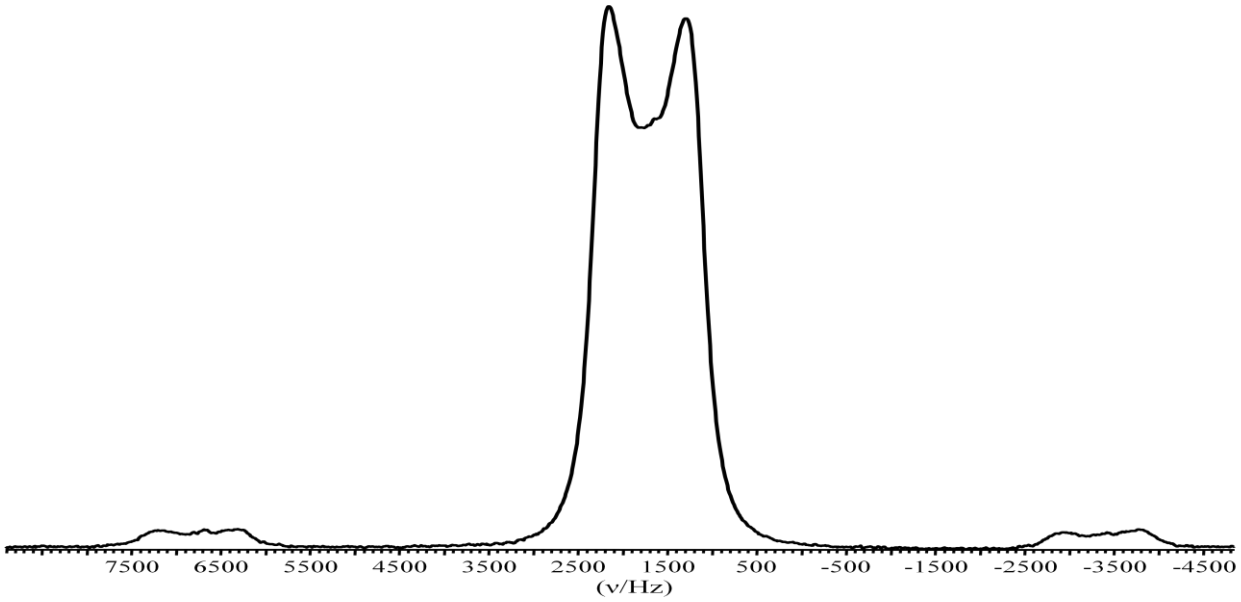

Fig. 4.2. ^{31}P NMR CP/MAS spectrum of tppAuCl at 4.70 T spinning at 5 kHz with spinning sidebands on either side of the central peaks after 1768 scans.

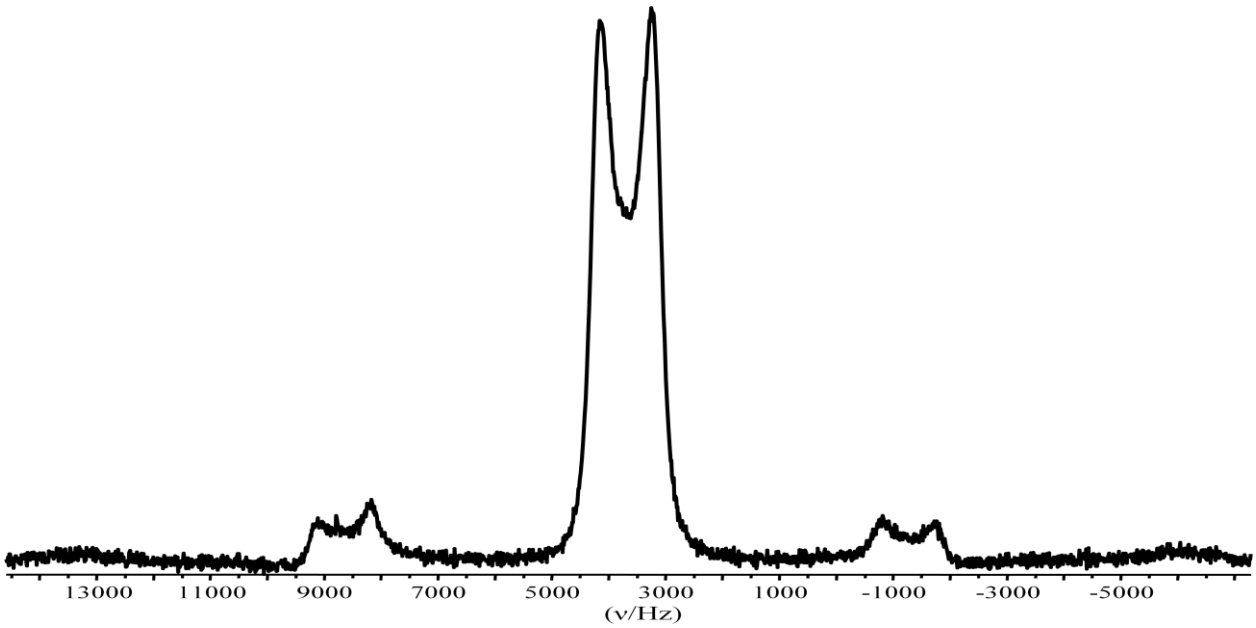

Fig. 4.3. ^{31}P CP/MAS spectrum of tppAuCl at 7.05 T spinning at 5 kHz with ssbs after 142 scans.

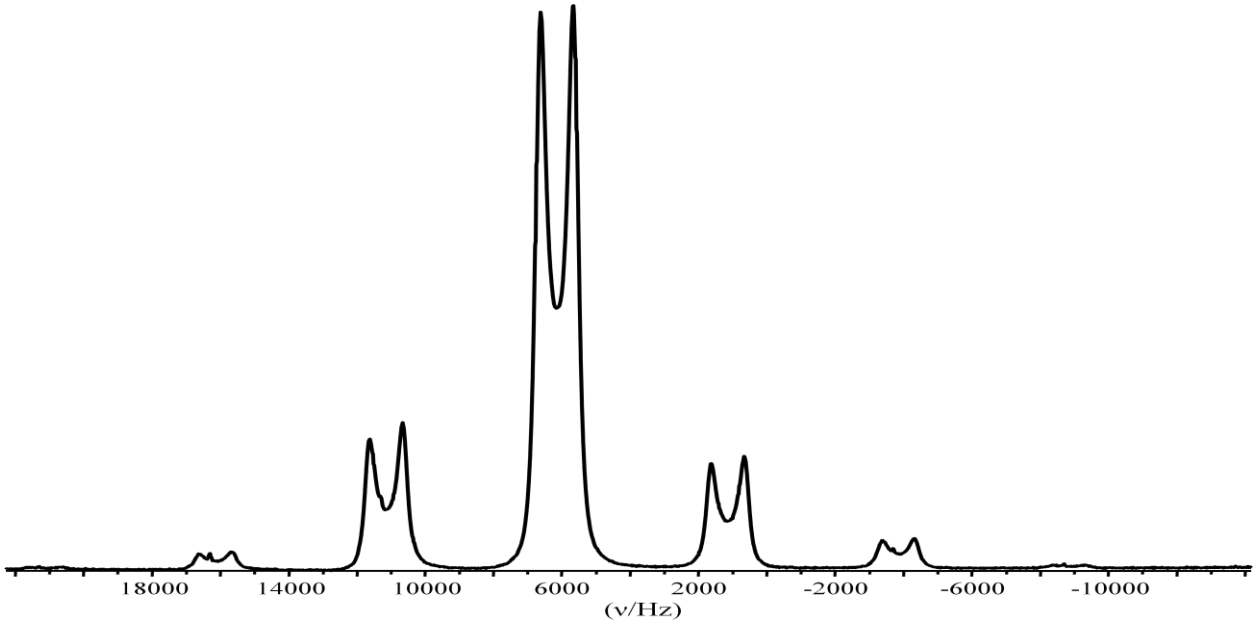

Fig. 4.4. ^{31}P CP/MAS spectrum of tppAuCl at 11.75 T spinning at 5 kHz after 1000 scans.

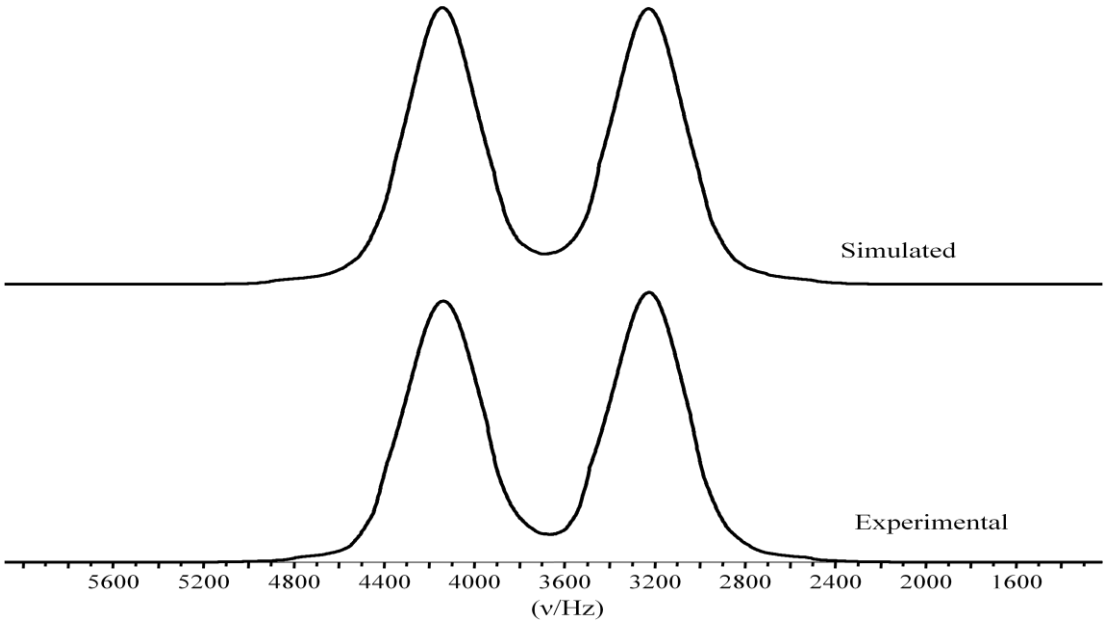

Fig. 4.5. Comparison of the experimental spectrum for tppAuCl acquired at 11.75 T with that calculated using WSOLIDS.

4.2 Chloro [1,1'-biphenyl-2-yl)di-tert-butylphosphine] gold(I) ((tbut)AuCl)

Chloro [1, 1'-biphenyl-2-yl) di-tertbutyl phosphine] gold(I) was studied using ^{31}P CP MAS NMR spectroscopy in the solid state at three fields: 4.70, 7.05, and 11.75 T.

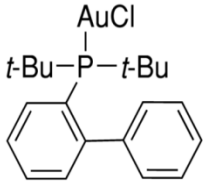

Fig. 4.6. Structure of tbutAuCl.

The acquired spectra can be seen below (*Figs.* 4.7, 4.8, and 4.9, respectively). At the field strengths of 7.05 T and 11.75 T, an asymmetric doublet was observed at 61 ppm. At a field strength of 4.70 T, a singlet was observed at 61 ppm. In either case, the spectra observed are made up of powder patterns. The splitting observed at the two higher field strengths are on the order of 1 kHz. It should also be noted that despite tripling the spinning frequency, a singlet was still observed at the 4.70 T magnetic field strength. The splitting is asymmetric due to the EFG tensor not being axially symmetric ($\eta_Q \neq 0$). Another reason could be that, due to the dependence of ^{197}Au's T_1 relaxation time on B_0, the relaxation time of ^{197}Au could be too short to be observed at the lower field strength. From using the aforementioned relationship between the splitting of the doublets and the indirect coupling constant that indicates the splitting is approximately 1.65 times the indirect coupling constant, the ^1J (^{197}Au, ^{31}P) was determined to be about 520 Hz. No value has been reported for (tbut)PAuCl in the literature as of this writing.

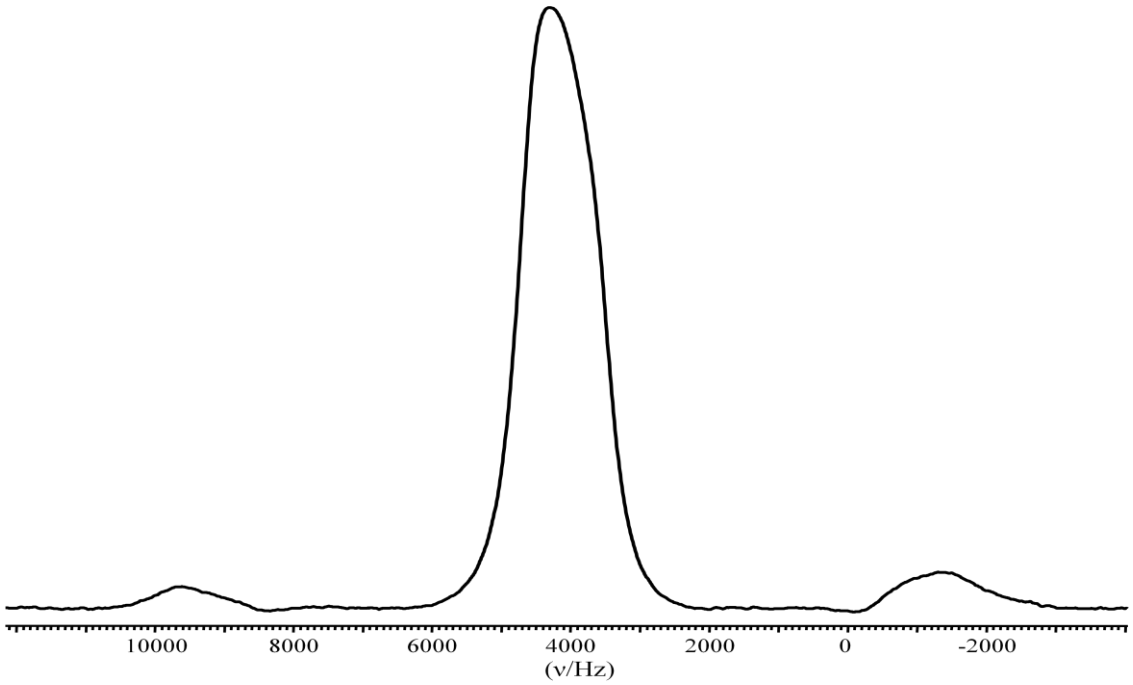

Fig. 4.7. ^{31}P CP/MAS spectrum of tbutAuCl at 4.70 T spinning at 5 kHz with ssbs after 8839 scans.

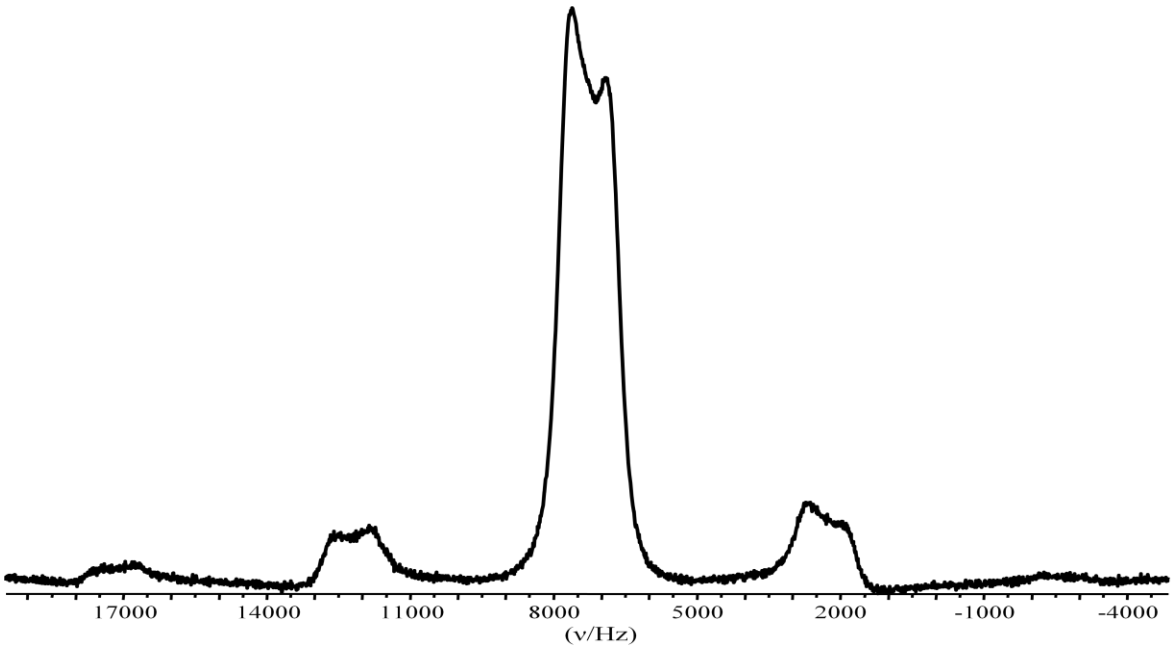

Fig. 4.8. ^{31}P CP/MAS spectrum of tbutAuCl at 7.05 T spinning at 5 kHz after 643 scans.

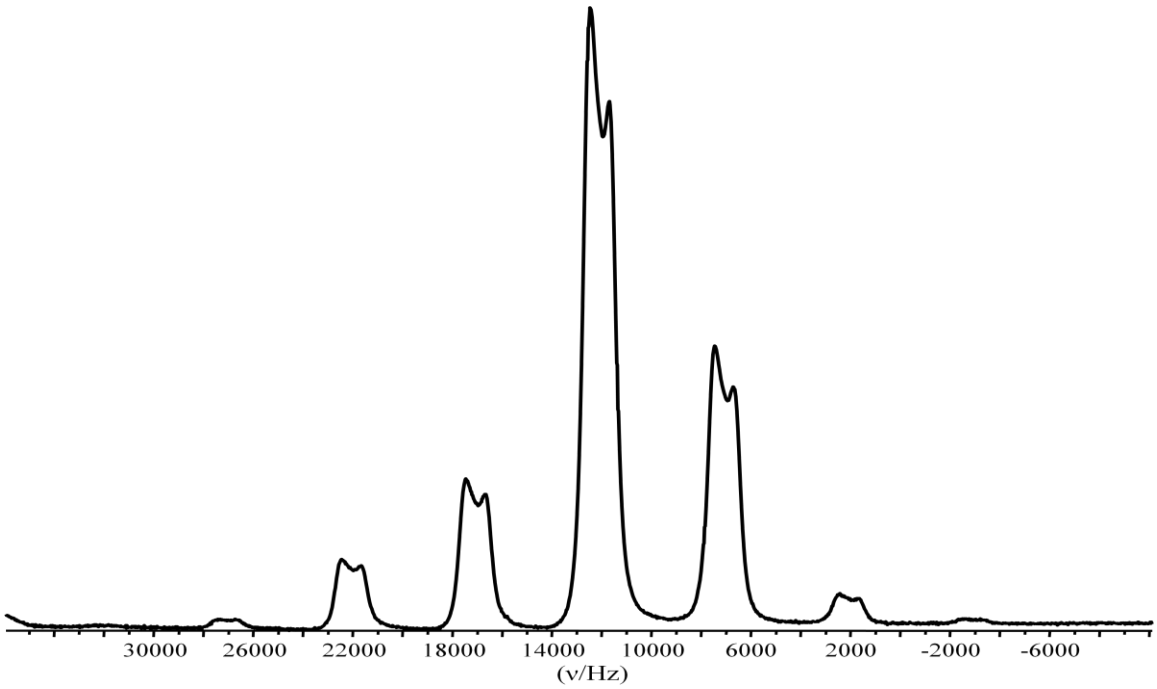

Fig. 4.9. ^{31}P CP/MAS spectrum of tbutAuCl at 11.75 T spinning at 5 kHz after 1000 scans.

4.3 Bis (chlorogold(I)) bis(diphenylphosphino) methane (((dppm)AuCl)$_2$)

Bis (chlorogold(I)) bis (diphenylphosphino) methane was studied using ^{31}P CP MAS NMR spectroscopy in the solid-state at three different fields: 4.70, 7.05, and 11.75 T. The spectra acquired at all three fields can be seen below (*Figs.* 4.11, 4.12, 4.13/4.14, respectively).

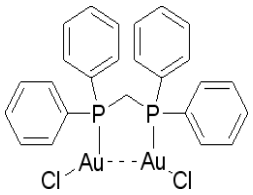

Fig. 4.10. Structure of $((dppm)AuCl)_2$.

At all three field strengths used to study $((dppm)AuCl)_2$, a symmetric doublet was observed at 28 ppm. The symmetric doublet is comprised of two sets of superimposed powder patterns, which can be seen in the simulated representations of the experimental spectra discussed later. The NMR experiments that were conducted to study $((dppm)AuCl)_2$ involved long pulse delays of 600 seconds and therefore the spectrometers were allowed to acquire the spectra for about a week. The splitting between the peaks of the doublet was determined to be about 1 kHz and did not change with a change in magnetic field strength. Again, this shows that the quadrupolar coupling interaction is so much larger than the Zeeman interaction that despite going to even higher fields, the spectrometer would not be able to resolve the signals enough to observe the expected quartet. From this splitting, the indirect coupling constant was determined to be 630 Hz. Through the use of the simulation program WSOLIDS, the experimentally determined indirect coupling constant between the ^{197}Au and ^{31}P was verified as being 630 Hz. No value for ^{1}J (^{197}Au, ^{31}P) has been reported in the literature for this compound as of this writing, however, one would expect that it would be on the same order as that for tppAuCl or analogues of this due to the similarities in the local environment about the phosphorus in these complexes. The ^{1}J(^{197}Au, ^{31}P) values in these types of gold phosphine halides can range from 510 to 650 Hz.[38]

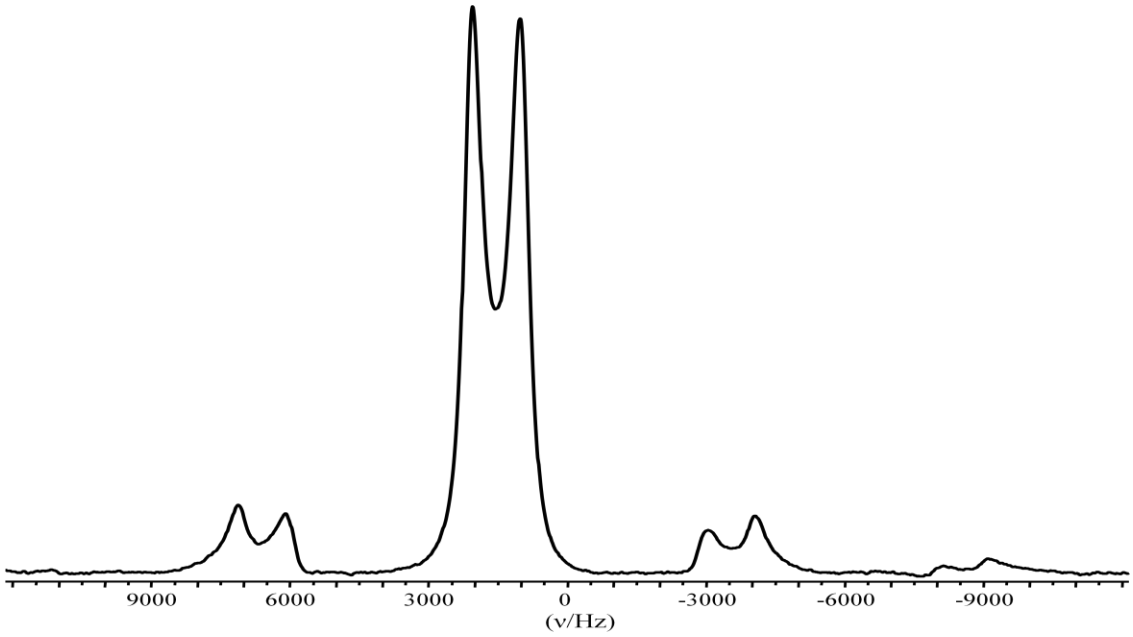

Fig. 4.11. ^{31}P CP/MAS spectrum of dppmAuCl$_2$ at 4.70 T spinning at 5 kHz after 1164 scans.

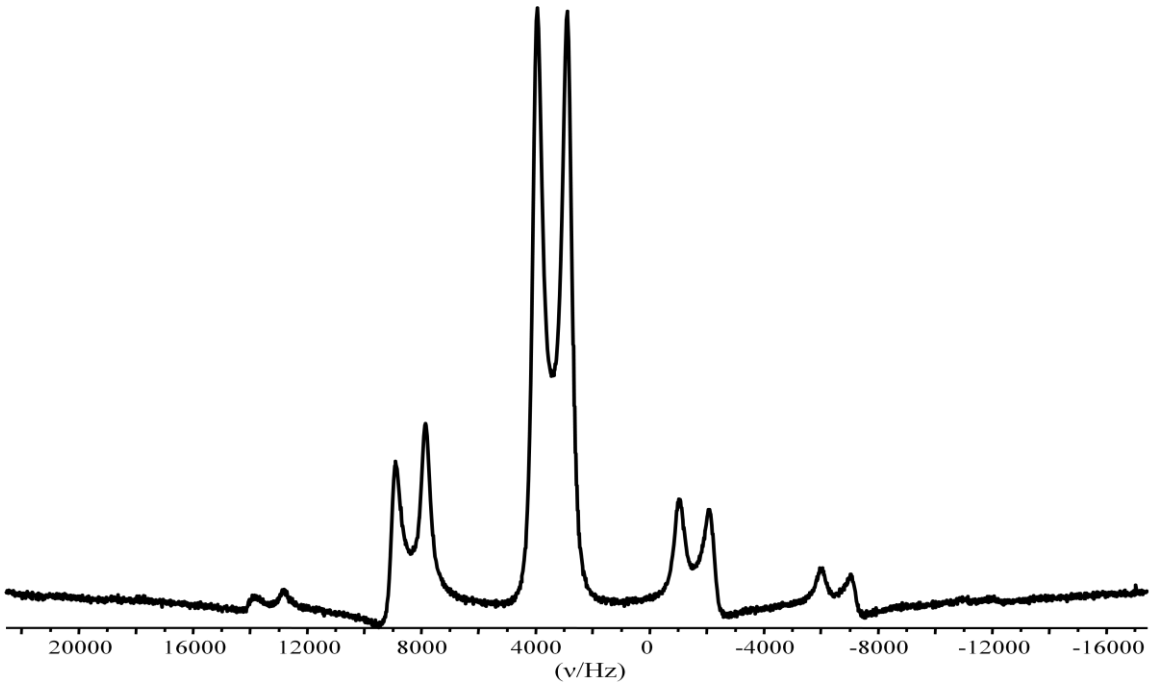

Fig. 4.12. ^{31}P CP/MAS spectrum of dppmAuCl$_2$ at 7.05 T spinning at 5 kHz after 142 scans.

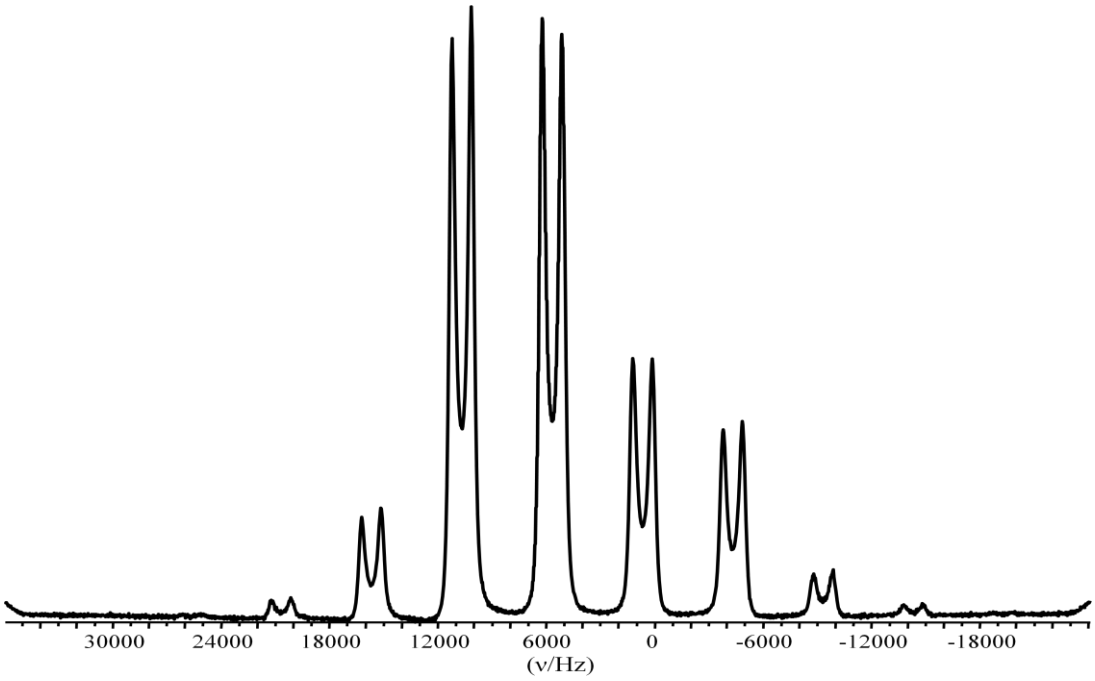

Fig. 4.13. ^{31}P CP/MAS spectrum of dppmAuCl$_2$ at 11.75 T spinning at 5 kHz after 1000 scans.

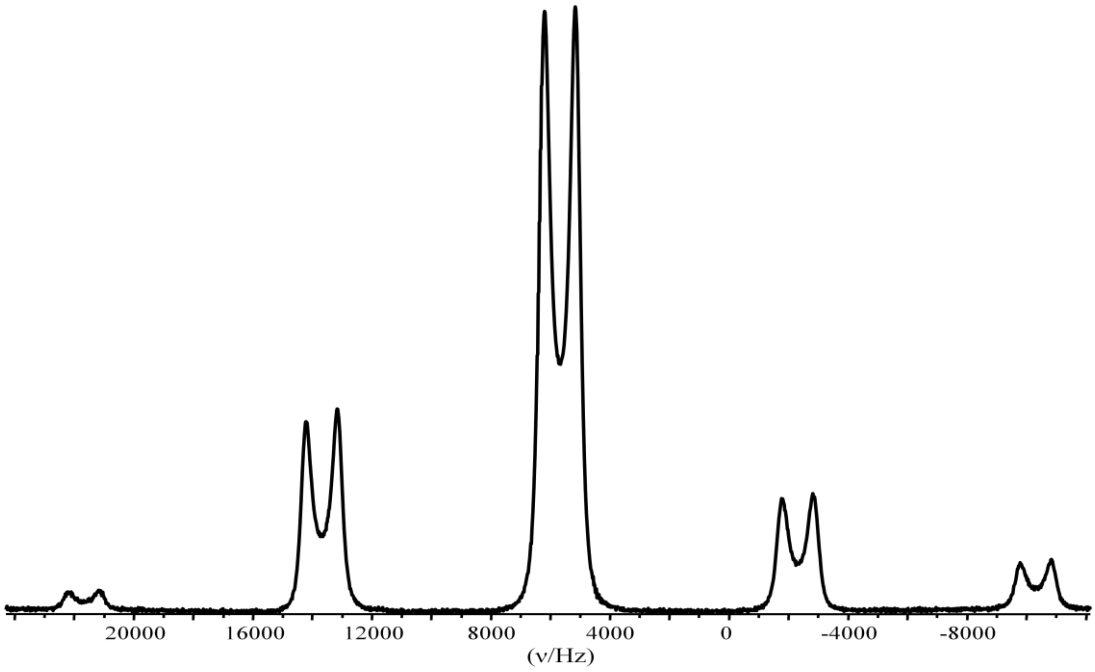

Fig. 4.14. ^{31}P CP/MAS spectrum of dppmAuCl$_2$ for 11.75 T spinning at 8 kHz after 128 scans.

For these simulations, the literature value for the quadrupolar coupling constant of gold was used (940 MHz).[2] A dipolar coupling constant of 76 Hz was calculated using the bond length between the ^{197}Au and ^{31}P (2.235 Å).[40,41] A line broadening of 380 Hz at 50% Lorentzian and 50% Gaussian was used to ensure the simulated spectrum was of the same breadth as that of the experimental spectrum. If no line broadening was introduced into the simulations, then only the overlapping powder patterns would be observed and not the broad peaks of the symmetric doublet as is observed in the experimental spectra. Euler angles of $\alpha = 0^0$ and $\beta = 0^0$ were used and indicate that the largest component of the electric field gradient tensor is along the bond axis of the ^{197}Au and ^{31}P bond. The value for η_Q was set to 0 and this means an axially symmetric EFG tensor. No literature value was found for this complex but since a singlet was observed for the reported NMR results for the triclinic polymorph of $((dppm)AuCl)_2$,[41] it is deduced that the monoclinic form, space group C2/c is the dominant one in this study.[42] The ^{31}P NMR spectrum acquired at 11.75 T and spinning at 5 kHz (*Fig.* 4.13) resulted in one of the spinning sidebands having equal intensity to the isotropic peak, this is due to the spinning speed not being fast enough to eliminate the CSA contribution to the spectrum, therefore a spectrum was acquired while spinning at 8 kHz (*Fig.* 4.14) and the CSA contribution was averaged.

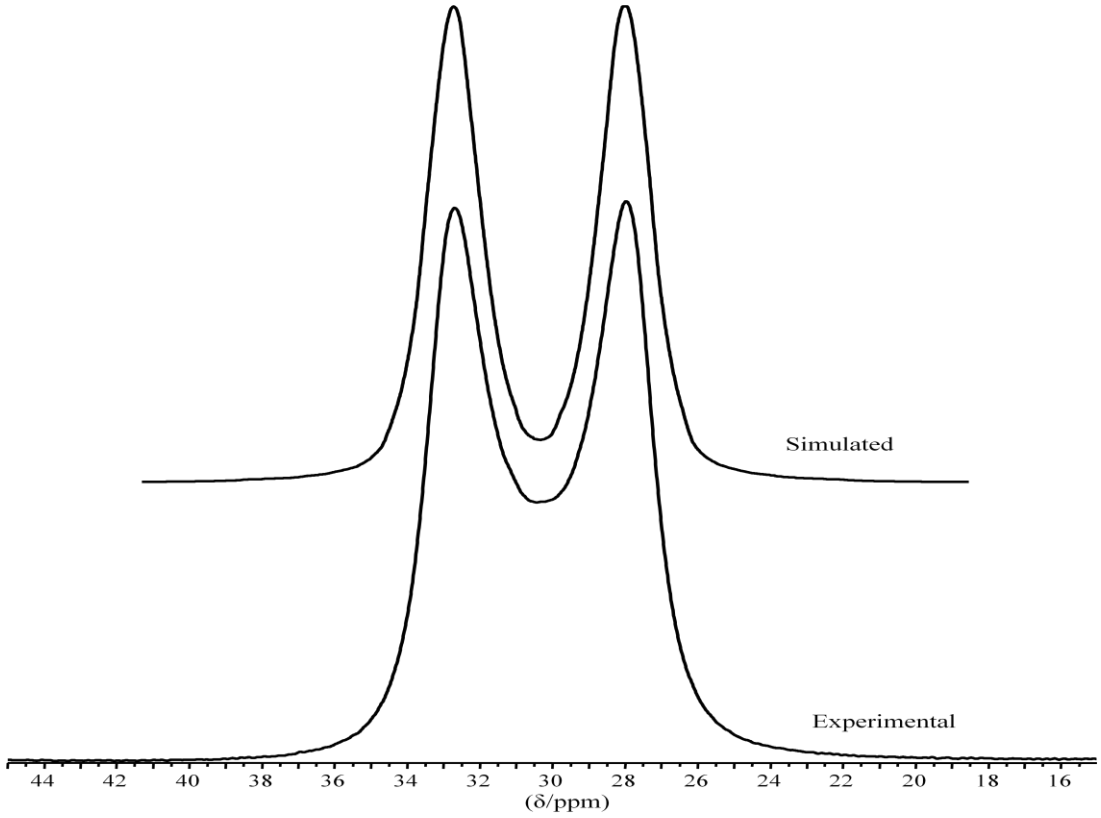

Fig. 4.15. Comparison of simulated spectrum with experimental spectrum of dppm$AuCl_2$ at 11.75 T.

4.4 Dichloro bis[(diphenylphosphino) ethane] digold (DPPEAuCl)

Dichloro bis[(diphenylphosphino) ethane] digold has been studied using ^{31}P CP MAS NMR spectroscopy in the solid state using a magnetic field strength of 11.75 T. The spectra for this complex are shown in *Fig.* 4.17 and 4.18. In the spectra, a singlet is observed.

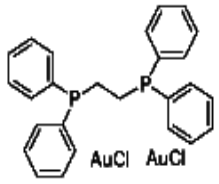

Fig. 4.16. Structure for DPPEAuCl.

This is the only gold complex studied for this research that gave a singlet at this field strength. The reason that a singlet was observed for DPPEAuCl at 11.75 T is most likely due to the rapid relaxation of the ^{197}Au. Performing variable temperature (VT) NMR experiments (i.e., going to lower temperatures) can decrease the relaxation rate enough so that spin-spin indirect coupling can be observed provided a low enough temperature can be attained. Therefore, VT experiments were undertaken to determine if indirect spin-spin coupling between ^{197}Au-^{31}P could be observed for this complex (*Fig.* 4.17). During these experiments, temperatures as low as 136 K were attained and at approximately 180 K, the first signs of indirect spin-spin coupling between ^{197}Au and ^{31}P could be observed. The spectra obtained at 150 K or lower resembled those obtained for the aforementioned gold complexes with a doublet appearing at approximately 30 ppm and a splitting on the order of 700 Hz. Recycle delays of 15 seconds were used during these experiments. The ^{1}J (^{197}Au, ^{31}P) value was determined from the line splitting in the low temperature spectrum at 136 K to be 420 Hz.

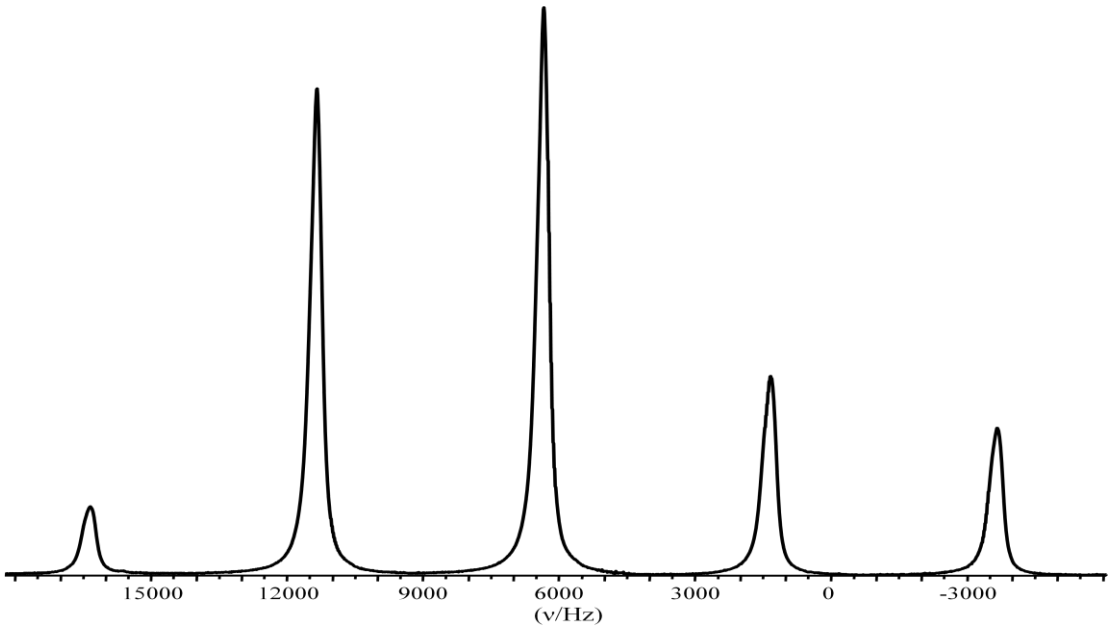

Fig. 4.17. ^{31}P CP/MAS spectrum of DPPEAuCl at 11.75 T spinning at 5 kHz after 3952 scans.

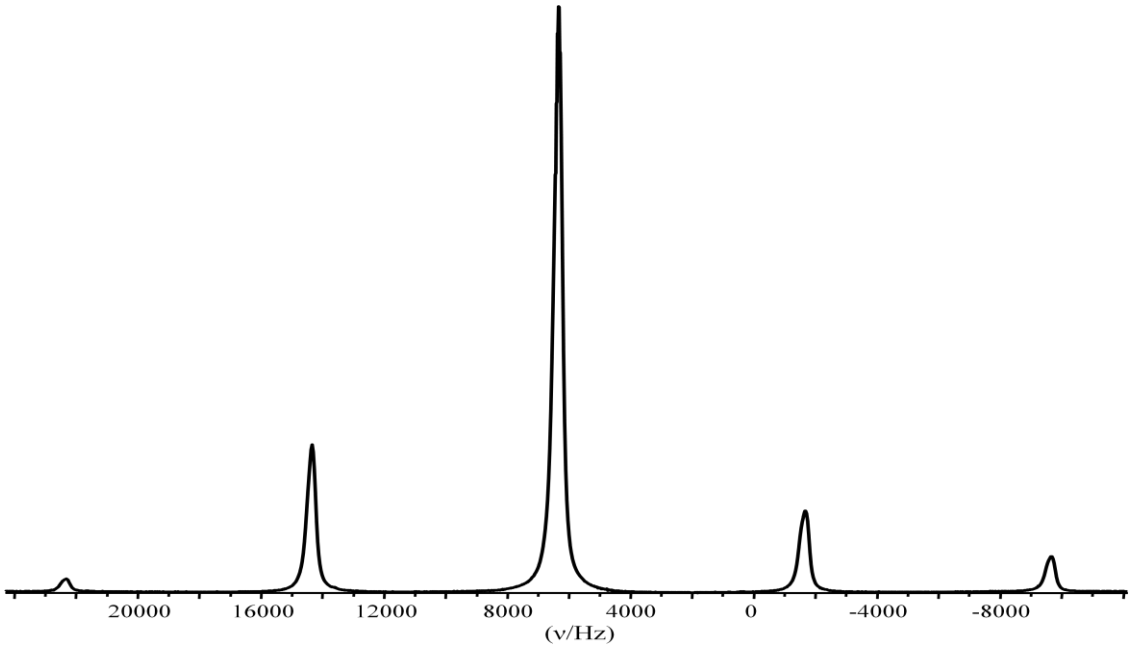

Fig. 4.18. ^{31}P CP/MAS spectrum of DPPEAuCl at 11.75 T spinning at 8 kHz after 5436 scans.

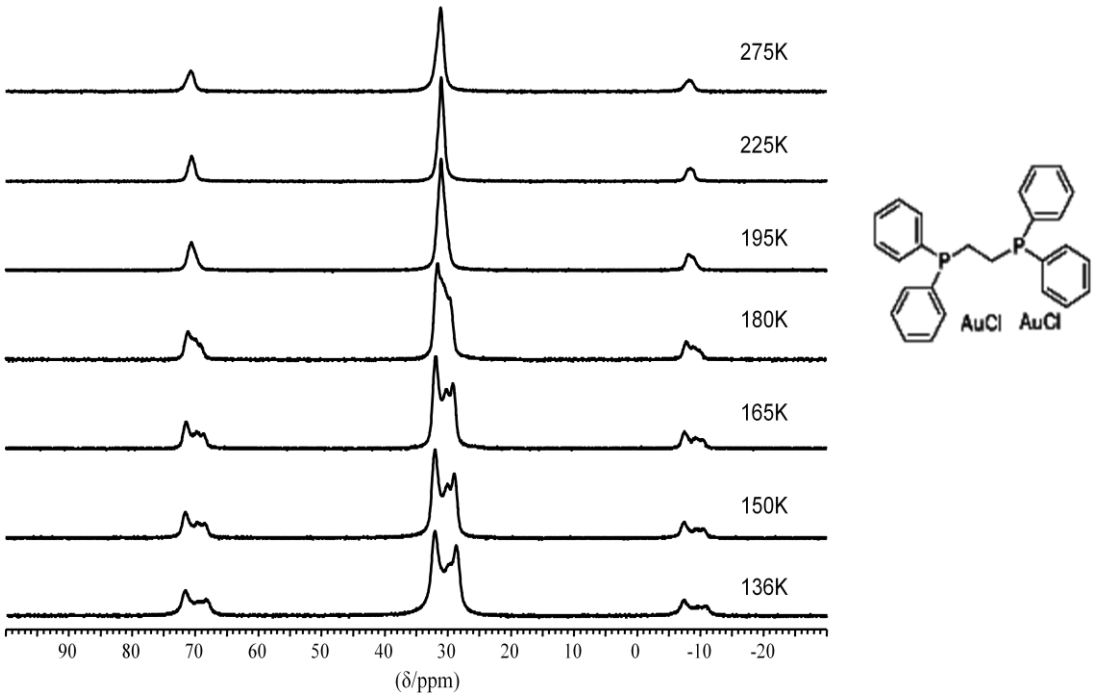

Fig. 4.19. ^{31}P CPMAS spectra of DPPEAuCl at 11.75 T at variable temperatures and spinning at 8 kHz for 4 scans at each temperature.

4.5 Triphenylphosphite gold(I) chloride ($(PhO)_3PAuCl$)

Solid triphenlyphosphite gold(I) chloride[43] was studied using ^{31}P CP MAS and stationary NMR spectroscopy at 14.09 T. It was the only gold phosphite complex studied for this research and yielded results quite different from those from the gold phosphine complexes studied.

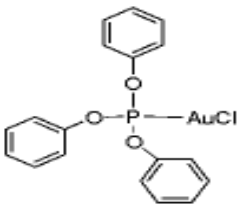

Fig. 4.20. Structure of $(PhO)_3PAuCl$.

At 14.09 T, a chemical shift anisotropy (CSA) pattern is observed over a range of –150 ppm to 100 ppm at a MAS rate of 11 kHz. The range of the CSA pattern at 5 kHz is about the same but with a greater number of peaks being observed. Recycle delays of 300 seconds were used during these experiments with ($\pi/2$) time of 2.25 μs. The crystals are triclinic, space group P1, with two molecules in the unit cell. Using a Herzfeld-Berger Analysis,[26] the principal components of the chemical shift tensor were calculated and indicated that the magnetic shielding tensor was axially symmetric. The chemical shift tensor values are as follows: $\delta_{11} = \delta_{22} = 86.5$ ppm, $\delta_{33} = -139.98$ ppm.

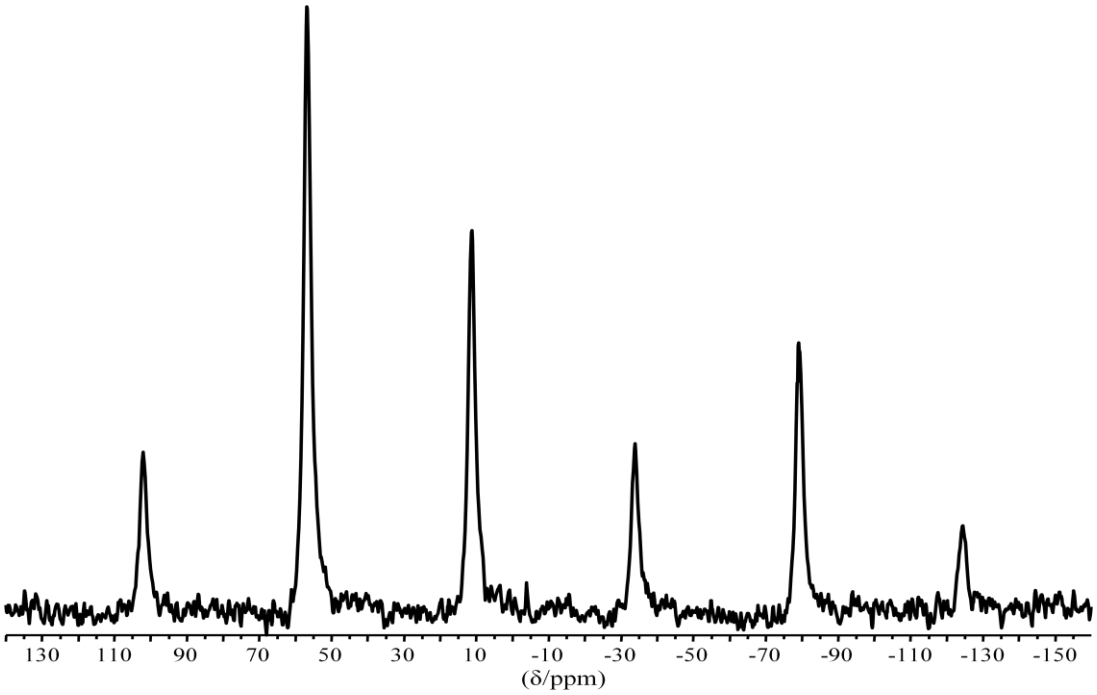

Fig. 4.21. ^{31}P CP/MAS spectrum of $(PhO)_3PAuCl$ at 14.09 T spinning at 11 kHz.

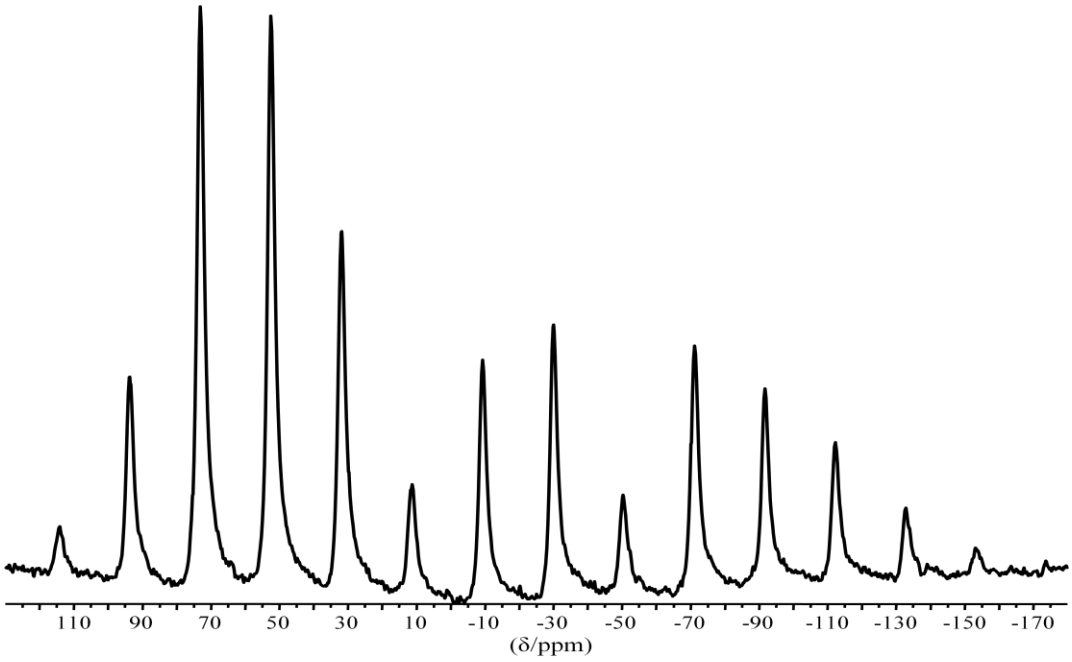

Fig. 4.22. ^{31}P CP/MAS spectrum of $(PhO)_3PAuCl$ at 14.09 T spinning at 5 kHz.

4.6 ADF Calculation Results

ADF calculations of the largest value of the EFG (q_{ZZ}) tensor were compared (see *Table 4.2*) on various simple gold halides with its known calculated literature values from microwave spectroscopy.[44,45]

Table 4.2. ADF Calculation Results for EFG (q_{zz}) at Gold (a.u.) using TZ2P basis set (QZ4P for AuH).

Method	AuF	XeAuF	KrAuF	ArAuF	(OC)AuF	AuH
Belpassi *et al.*[44]	-0.394	-4.39	-3.37	-2.65	-8.24	1.61
MPW1PW	-0.392	-4.57	-3.60	-2.77	-9.16	1.18
B1PW91	-0.404	-4.60	-3.63	-2.80	-9.19	1.16
PBE0	-0.420	-4.61	-3.63	-2.81	-9.19	1.17
B1LYP	-0.083	-4.32	-3.32	-2.49	-8.91	1.43
X3LYP	0.223	-4.05	-3.04	-2.21	-8.62	1.65
B3LYP	0.374	-3.92	-2.92	-2.08	-8.48	1.74
B3LYP*	0.868	-3.50	-2.48	-1.64	-8.04	2.07
O3LYP	1.06	-3.17	-2.15	-1.32	-7.61	2.39
OPBE0	-1.04	-5.09	-4.16	-3.36	-9.66	0.684
BHandHLYP	-2.48	-6.31	-5.37	-4.59	-11.0	-0.199
BHandH	-2.29	-6.15	-5.20	-4.41	-10.9	0.053
KMLYP	-2.99	-6.72	-5.80	-5.03	-11.4	-0.509
mPW1K	-2.11	-6.02	-5.09	-4.30	-10.7	-0.010

The functional and basis set were selected based on the combination which best agreed with the values for q_{ZZ} given by Belpassi *et al.*[44] The best combination was found to be to use the hybrid B1LYP as the functional and a triple zeta basis function with 2 polarized orbitals (TZ2P) with an integration of 8. (See Appendix for sample input files)

The Zeroth Order Relativistic Approximation (ZORA)[46] was used to account for any relativistic effects due to the presence of the gold nucleus. This setup involving the B1LYP functional and the triple zeta basis set (quadruple zeta basis set for AuH) resulted in the best agreement with the literature values obtained by Belpassi *et al.*[44] This combination was then used to calculate the nuclear quadrupolar coupling constant of the same simple gold halides to determine how accurately it compared to the literature values (see *Table 4.3*). A quadrupole moment value of 510 millibarns[44] (mb) was used to calculate C_Q from q_{zz} using *Equation* 2.15.

Table 4.3. ADF Calculation Results for C_Q (^{197}Au) Values (MHz).

C_Q values	AuF	XeAuF	KrAuF	ArAuF	(OC)AuF	AuH
Experimental[47,48,49,50]	-53.2	-527	-404	-323	-1006	187
Belpassi	-48.3	-539	-414	-326	-1011	197
Error (%)	9.21	2.22	2.29	0.700	0.460	5.53
B1LYP	-10.3	-529	-407	-306	-1092	175
Error (%)	80.7	0.430	0.660	5.45	8.57	6.16

This combination was then used to calculate the indirect spin-spin coupling constants for the gold phosphine halide complexes. This combination (B1LYP/ZORA) was then modified since NMR calculations using hybrid functionals are not supported by ADF. Therefore, the TZ2P and QZ4P basis sets were used in addition to ZORA based on how they agreed with the indirect coupling constant values reported in the literature. Values for the indirect

coupling constant were found to be in good agreement with literature values determined by other computation programs, such as Gaussian.[51]

NMR calculations of *J* were undertaken using the ADF program. The calculations were performed on phosphine gold chloride, triphenylphosphine gold chloride, trimethylphosphine gold chloride, trimethylphosphine gold bromide, and trimethylphosphine gold iodide. The determined experimental values of *J* given for the aforementioned gold phosphine complexes can be found in *Table 4.4*, as well as the results of the ADF calculations of *J* for the gold phosphine complexes. For triphenylphosphine gold chloride, these calculations predict that $J_{\parallel}$ and $J_{\perp}$ have values of 610 and 382 Hz, respectively, for a J_{iso} value of 458 Hz and ΔJ value of 228 Hz. The ADF calculations predict $^{1}J(^{197}\text{Au}, ^{31}\text{P})$ to be positive.

Table 4.4. ADF Results for *J*-coupling for gold phosphine halides.

Molecule	Experimental (Hz)[4]	Computational (Hz)
$(PH_3)AuCl$	--	323
$(PMe_3)AuCl$	648	753
$(PMe_3)AuBr$	--	412
$(PMe_3)AuI$	553	596
$(PPh_3)AuCl$	521[37]	458

NMR calculations were also performed on trimethylphosphine gold chlorides as a function of ^{197}Au-^{31}P bond length to determine the relationship between bond length and *J*-coupling value, see *Table 4.5* and *Fig. 4.23*. The structure used was based on the crystal structure given by Angermair *et al.*[4]

Table 4.5. ADF Results for effect of ^{197}Au-^{31}P bond length (in Å) on *J* (in Hz) in (PMe_3)AuCl.

^{197}Au-^{31}P Bond length	$^{1}J(^{197}$Au-^{31}P)
2.134	860
2.224	760
2.234	750
2.244	740
2.334	650

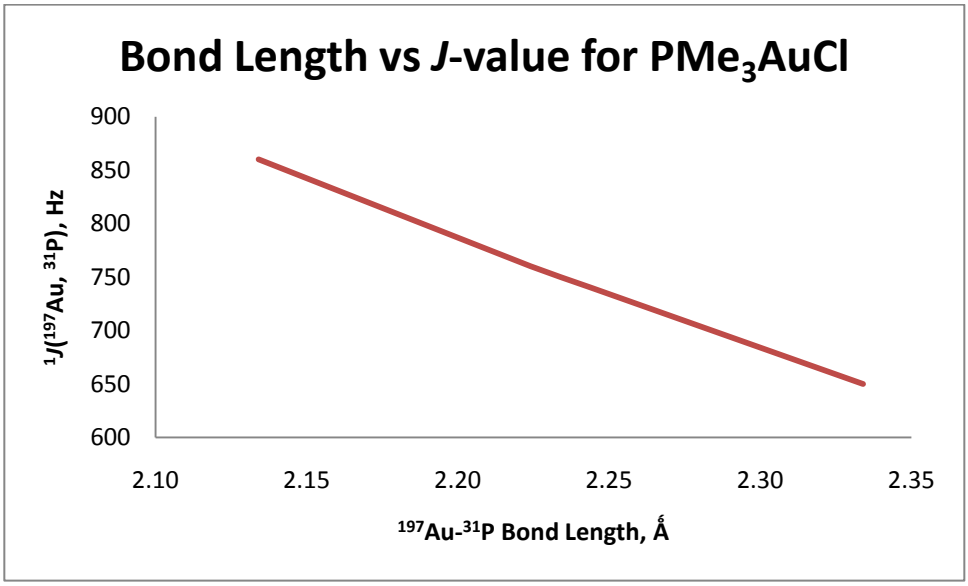

Fig. 4.23. Plot of ^{197}Au-^{31}P bond length and $^{1}J(^{197}$Au, ^{31}P).

The agreement between experimental and computational results is very good varying at most by 16%. A trend was noted for the calculations involving varying ^{197}Au-^{31}P bond lengths; as the bond length increases the value of *J* decreases, thus resulting in a *J* value shift of approximately 1000 Hz Å^{-1}. The

change in the value of the reduced coupling constant, *K*, was also determined by calculating the *K* values from the *J* values determined for the different ^{197}Au-^{31}P bond lengths.

$$K(I,S) = \frac{J(I,S)\ 4\pi^2}{h\gamma_I\gamma_S} \qquad (3.1)$$

where *h* is Planck's constant.

These *K* values were also then compared with the *K* values calculated for ^{109}Ag-^{31}P as was determined previously by former Wasylishen group member, Dr. Fu Chen (see *Table* 4.6).[52] The K values for ^{197}Au-^{31}P were found to be larger than those for ^{109}Ag-^{31}P. This was done to determine any evidence of a periodic trend; as you move down the column, the change in value increases (*Table* 4.7).

Table 4.6. Comparison of Δ*J* (Hz) and ΔK (kgm^{2}s^{2}Å^2) values for ^{197}Au-^{31}P, and ^{107}Ag-^{31}P.

M-P bond	Δ*J*	ΔK
^{107}Ag-^{31}P	180	7.9E+21
^{197}Au-^{31}P	200	-2.2E+22

Table 4.7. Comparison of Δ*J* (Hz) and ΔK (kgm^{2}s^{2}Å^2) values for ^{197}Au-^{31}P, ^{107}Ag-^{31}P, ^{65}Cu-^{31}P using *J*-values of 550 and 1000 Hz.

M-P bond	Δ*J*	ΔK
^{65}Cu-^{31}P	450	32.52E+20
^{107}Ag-^{31}P	450	197.6E+20
^{197}Au-^{31}P	450	522.8E+20

Chapter 5:

Conclusions

The research that has been presented in this thesis was done with the purpose of improving the ability to extract NMR parameters, specifically the indirect coupling constant, and to investigate and compare different gold-phosphine halides using solid-state ^{31}P CP MAS spectra under the condition of having a system where the quadrupolar coupling interaction is much greater than the Zeeman interaction. The other purpose of this research was to prove that solid-state NMR is a viable method to extract spectral parameters for gold phosphine halides and that with the combination of simulations and calculations, it can be a powerful method of investigation. The results of the experiments undertaken for the purposes of this thesis are summarized below as well as some points of discussion and recommendations to potentially further the research in this field of study. This summary begins with a discussion on the NMR experiments conducted, then moving on to the simulations and calculations that were performed to aid in spectral analysis, and finally ending with a review of the results that were acquired from the combination of simulation and experimental.

Through the use of WSOLIDS, the acquired spectra for the gold phosphine halides were simulated. These simulations were useful for helping to extract the indirect coupling constant values from the experimental spectra and the values given from the simulations were complementary to those taken directly from the spectra. In addition to the simulations performed using WSOLIDS, ADF

DFT calculations were performed on the complexes as well as several simple gold halides; these gold halide complexes as well as the ones that were the subject of this thesis were previously only studied using Gaussian DFT if at all.

The ^{31}P CP MAS NMR spectra acquired for triphenyl phosphine gold(I) chloride yielded a symmetric doublet at all three field strengths used. The line splitting was determined to be on the order of 1 kHz and this line splitting was further used to calculate a $^{1}J(^{197}\text{Au}, ^{31}\text{P})$ value of 550 Hz. The spectra for triphenyl phosphine gold(I) chloride were then simulated using values from the literature as well as structural information and these simulations gave a $^{1}J(^{197}\text{Au}, ^{31}\text{P})$ value of 550 Hz as well. This value was found to be in good agreement with the literature value of 520 Hz that was previously reported.[38]

The ^{31}P CP MAS NMR spectra that were acquired for chloro [1,1'-biphenyl-2-yl] (di-tertbutyl phoshphine) gold(I) gave an asymmetric doublet at the two highest field strengths and a singlet at the lowest field strength. The line splitting was used to determine the $^{1}J(^{197}\text{Au}, ^{31}\text{P})$ value of 520 Hz. The spectra were then simulated using WSOLIDS from literature values and using structural information. These simulations yielded an indirect coupling constant of 530 Hz. No literature value was found for this complex but it seems to be in agreement with what would be expected given the local environment of the ^{31}P nucleus.

The ^{31}P CP MAS NMR spectra acquired for bis (dichloro gold(I)) bis (diphenylphosphino) methane gave a symmetric doublet at all field strengths studied. From the line splitting, a $^{1}J(^{197}\text{Au}, ^{31}\text{P})$ value of 630 Hz was calculated.

The subsequent simulations gave the same value for the indirect coupling constant. No literature value was found for this complex but since a singlet was observed for the reported NMR results for the triclinic polymorph of $((dppm)AuCl)_2$,[41] it is deduced that the monoclinic form is the dominant one in this study. The calculated indirect coupling constant seems to be on par with other gold phosphine halides that exhibit a similar local geometry.

The ^{31}P CP MAS NMR spectra acquired for dichoro (diphenylphosphino ethane) digold(I) gave a singlet at room temperature at 11.75 T (no other field strengths were studied). Through the use of variable temperature ^{31}P CP MAS NMR, a doublet was observed at 136 K and a ^{1}J value of 420 Hz was calculated from the line splitting. No literature value was found for this complex.

The ^{31}P CP MAS NMR spectra acquired for (triphenylphosphite) gold(I) chloride gave a CSA pattern with δ_{iso} showing at ~10 ppm. A stationary sample ^{31}P CP spectrum was also acquired which gave an asymmetric powder pattern. No simulations were performed on this sample as of yet and no literature values for ^{1}J were found for this complex.[43]

The $^{1}J(^{197}Au, ^{31}P)$ values have been measured experimentally and calculated using modern quantum chemistry (ADF) calculations. These DFT calculations have been able to reproduce experimental trends as was observed for the EFGs for ^{197}Au and $^{1}J(^{197}Au, ^{31}P)$. Relativistic effects appear to be important in the reproduction of these trends as non-relativistic calculations introduced a larger margin of error. For triphenylphosphine gold chloride, these calculations

predict that $J_{\parallel}$ and $J_{\perp}$ have values of 610 and 382 Hz, respectively, for a J_{iso} value of 458 Hz and ΔJ value of 228 Hz. The DFT calculations predict $^{1}J(^{197}\text{Au}, ^{31}\text{P})$ to be positive and this agrees with what has been calculated experimentally.

Hopefully with the help of this research, many similar complexes (where the quadrupolar coupling interaction is much larger than the Zeeman interaction) can be studied in a similar manner and this research can further be applied to other areas. A possible suggestion would be to apply these experiments on the copper and silver analogues of the gold phosphine halides studied to determine how the indirect coupling constant values change by changing the metal within a column of the periodic table. Another suggestion would be to further attempt to observe a doublet at 4.70 T for (tbut)PAuCl by conducting variable temperature NMR experiments at low temperatures to slow down the fast relaxation of this complex due to the internal rotation of the tert-butyl groups bonded to the phosphorus.

References

1. Pyykkö, P., *Mol. Phys.*, 106 (**2008**), 1965-1974.
2. Maddock, A.G., Jones, P.G., Mays, M.J., Muir, M.M., Williams, A.F., *J. Chem. Soc., Dalton Trans.*, (**1977**), 1434-1439.
3. Harris, R.K. *Nuclear Magnetic Resonance Spectroscopy*; Longman Group UK Limited, 1987.
4. Angermair, K., Bowmaker, G.A., de Silva, E.N., Healy, P.C., Jones, B.E., Schmidbaur, H., *J. Chem. Soc. Dalton Trans.*, (**1996**), 3121-3129.
5. Haeberlen, U. *Advances in Magnetic Resonance, Suppl. 1: High Resolution NMR in Solids: Selective Averaging*; Academic Press: New York, 1976.
6. Menger, E.M., Veeman, W.S., *J. Magn. Reson.*, 46 (**1982**), 257-268.
7. Olivieri, A.C., *Solid State Nucl. Magn. Reson.*, 1(**1992**), 345-353.
8. Harris, R.K., Becker, E.D., Cabral de Meneses, S.M., Goodfellow, R., and Granger, P., *Solid State Nucl. Magn. Reson.*, 22 (**2002**), 458-483.
9. Ramsey, N.F., *Phys. Rev.*, (**1950**), *78*, 699-703.
10. Bernard, G.M., Eichele, K., Wu, G., Kirby, C.W., Wasylishen, R.E., *Can. J. Chem.*, 78 (**2000**), 614-625.

11. Proctor, W.G., Yu, F.C., *Phys. Rev.*, 77 (**1950**), 717.

12. Jameson, C.J., *Encyclopedia of Nuclear Magnetic Resonance*; Grant, D.M., R.K. Harris, Eds.; John Wiley and Sons, Ltd.: Chichester, 1996, pp 1278-1281.

13. Mehring, M. *Principles of High Resolution NMR in Solids; 2nd Ed.*; Springer-Verlag: Berlin, 1983.

14. Wasylishen, R.E., *Encyclopedia of Nuclear Magnetic Resonance*; Grant, D.M., R.K. Harris, Eds.; John Wiley and Sons, Ltd.: Chichester, 1996, pp1685-1695.

15. Gillespie, R.J., Granger, P., Morgan, K.R., Schrobilgen, G.J., *Inorg. Chem.*, 23 (**1984**), 887.

16. Chen, F., Wasylishen, R.E., *Magn. Reson. Chem.* 48 (**2010**), 270-275.

17. Nelson, J.H., *Conc. Magn. Reson.*, 14 (**2002**), 19-78.

18. Man, P.P, *Encyclopedia of Nuclear Magnetic Resonance*; Grant, D.M., Harris, R.K., Eds; John Wiley and Sons, Ltd.: Chichester, 1996, pp 3838-3848.

19. Vega, A.J., *Encyclopedia of Nuclear Magnetic Resonance*; Grant, D.M., Harris, R.K., Eds; John Wiley and Sons, Ltd.: Chichester, 1996, pp 3869-3889.

20. Olivieri, A.C., *J. Magn. Reson.*, 81 (**1989**), 201-205.

21. Zumbulyadis, N., Henrichs, P.M., Young, R.H., *J. Chem. Phys.*, 75 (**1981**), 1603-1611.

22. Hexem, J.G., Frey, M.H., Opella, S.J., *J. Chem. Phys.*, 77 (**1982**), 3847-3856.

23. Alarcon, S.H., Olivieri, A.C., Harris, R.K., *Solid State Nucl. Magn. Reson.*, 2(**1993**), 325-334.

24. Grondona, P., Olivieri, A.C., *Concepts in Magn. Reson.*, 5(**1993**), 319-339.

25. Bain, A.D., Khasawneh, M., *Concepts in Magn. Reson. A*, 22A (**2004**), 69-78.

26. Herzfeld, J., Berger, A.E., *J. Chem. Phys.*, 73 (**1980**), 6021-6030.

27. Maricq, M.M., Waugh, J.S., *J. Chem. Phys.*, 70 (**1979**), 3300-3316.

28. Engelke, F., *Encyclopedia of Nuclear Magnetic Resonance*; Grant, D.M., Harris, R.K., Eds; John Wiley and Sons, Ltd.: Chichester, 1996, pp 1529-1534.

29. Burum, D.P, *Encyclopedia of Nuclear Magnetic Resonance*; Grant, D.M., Harris, R.K., Eds; John Wiley and Sons, Ltd.: Chichester, 1996, pp 1535-1543.

30. Hartmann, S.R., Hahn, E.L., *Phys. Rev*., 128 (**1962**), 1-323.

31. Metz, G., Wu, X., Smith, S.O., *J. Magn. Reson. Ser. A*, 110 (**1994**), 219-227.

32. Olivieri, A.C., *J. Mag. Res.*, 101(**1992**), 313-316.

33. De Silva, E.N., Bowmaker, G.A., Healy, P.C., *J. Mol. Struct.*, 516 (**2000**), 263-272.

34. Faltens, M.O., Shirley, D.A., *J. Chem. Phys.*, 53 (**1970**), 4249-4264.

35. Theoretical Chemistry, Vrije Universiteit, Amsterdam, http://www.scm.com.

36. Bryce, D.L., Bernard, G.M., Gee, M., Lumsden, M.D., Eichele, K., Wasylishen, R.E., *Can. J. Anal. Sci. Spec.*, 46 (**2001**), 46-82.

37. Baker, L-J., Bowmaker, G.A., Healy, P.C., Skelton, B.W., White, A.H., *J. Chem. Soc. Dalt. Trans.*, 1 (**1992**), 989-997.

38. Borissova, A.O., Korlyukov, A.A., Antipin, M.Y., Lyssenko, K.A., *J. Phys. Chem. A*, 112 (**2008**), 11519-11522.

39. http://anorganik.uni-tuebingen.de/klaus/soft/index.php?p=wsolids1/wsolids1

40. Healy, P.C., *Acta Cryst. Sect. E*, E59 (**2003**), m1112-m1114.

41. Van Calcar, P.M., Olmstead, M.M., Balch, A.L., *Inorg. Chem.*, 36 (**1997**), 5231-5238.

42. Schmidbaur, H., Wohlleben, A., Wagner, F., Orama, O., Hunter, G., *Chem. Ber.*, 110 (**1977**), 1748-1754.

43. Hitchcock, P.B., Pye, P.L., *J. Chem. Soc., Dalton Trans.*, (**1977**), 1457-1460.

44. Belpassi, L., Tarantelli, A., Sgamellotti, A., Götz, A.W., Visscher, L., *Chem. Phys. Letters*, 442 (**2007**), 233-237.

45. Bryce, D.L., Wasylishen, R.E., *J. Chem. Ed.*, 78 (**2001**), 124-133.

46. Autschbach, J., Ziegler, T., *Encyclopedia of Nuclear Magnetic Resonance*: Grant, D.M., Harris, R.K., Eds.; John Wiley and Sons, Ltd.: Chichester, UK, 2002; Vol. 9, pp 306-323.

47. Cooke, S.A, Gerry, M.C.L., *J. Am. Chem. Soc.*, 126 (**2004**), 17000-17008.

48. Evans, C.J., Reynard, L.M., Gerry, M.C.L., *Inorg. Chem.*, 40 (**2001**), 6123-6131.

49. Evans, C.J., Rubinoff, D.S., Gerry, M.C.L., *Phys. Chem. Chem. Phys.*, 2 (**2000**), 3943-3948.

50. Evans, C.J., Gerry, M.C.L, *J. Am. Chem. Soc.*, 122 (**2000**), 1560-1561.

51. Gaussian 03, Revision C.02, Frisch, M. J.; Trucks, G. W.; Schlegel, H. B.; Scuseria, G. E.; Robb, M. A.; Cheeseman, J. R.; Montgomery, Jr., J. A.; Vreven, T.; Kudin, K. N.; Burant, J. C.; Millam, J. M.; Iyengar, S. S.; Tomasi, J.; Barone, V.; Mennucci, B.; Cossi, M.; Scalmani, G.; Rega, N.; Petersson, G. A.; Nakatsuji, H.; Hada, M.; Ehara, M.; Toyota, K.; Fukuda, R.; Hasegawa, J.; Ishida, M.; Nakajima, T.; Honda, Y.; Kitao, O.; Nakai, H.; Klene, M.; Li, X.; Knox, J. E.; Hratchian, H. P.; Cross, J. B.; Bakken, V.; Adamo, C.; Jaramillo, J.; Gomperts, R.; Stratmann, R. E.; Yazyev,

O.; Austin, A. J.; Cammi, R.; Pomelli, C.; Ochterski, J. W.; Ayala, P. Y.; Morokuma, K.; Voth, G. A.; Salvador, P.; Dannenberg, J. J.; Zakrzewski, V. G.; Dapprich, S.; Daniels, A. D.; Strain, M. C.; Farkas, O.; Malick, D. K.; Rabuck, A. D.; Raghavachari, K.; Foresman, J. B.; Ortiz, J. V.; Cui, Q.; Baboul, A. G.; Clifford, S.; Cioslowski, J.; Stefanov, B. B.; Liu, G.; Liashenko, A.; Piskorz, P.; Komaromi, I.; Martin, R. L.; Fox, D. J.; Keith, T.; Al-Laham, M. A.; Peng, C. Y.; Nanayakkara, A.; Challacombe, M.; Gill, P. M. W.; Johnson, B.; Chen, W.; Wong, M. W.; Gonzalez, C.; and Pople, J. A.; Gaussian, Inc., Wallingford CT, 2004.

52. Chen, F., Wasylishen, R.E., *Magn. Reson. Chem.*, 48 (**2010**), 270-275.

Appendix

A.1. ADF Input file for calculation of *J* for (PMe_3)AuCl

```
#!/bin/sh
cd PMeAuCl

$ADFBIN/adf -n 4 << eor

Atoms
Au       0.000000000      0.000000000      0.000000000
Cl       1.231289497      1.543728876     -1.198719038
P       -1.190779540     -1.492939528      1.159280663
C       -2.171546932     -2.722576381      2.114104485
H       -2.865472659     -2.232067067      2.789674269
H       -2.749946504     -3.361434788      1.453922213
H       -1.527104119     -3.361434788      2.709990513
End

relativistic spinorbit zora

symmetry NOSYM

qtens

XC
   lda vwn
   gga becke perdew
end

integration 8

Basis
   Type ZORA/QZ4P
   Core None
End

save TAPE10

End input
eor

$ADFBIN/cpl -n 4 <<eor
nmrcoupling
GAMMA 1 4730600
dso
pso
fc
sd
```

```
scf convergence 1e-5
nuclei 1 3
end
ENDINPUT
eor

rm TAPE21 logfile TAPE10
```

A.2. ADF Input file for calculation of J for (PPh_3)AuCl

```
#!/bin/sh
cd Ph3PAuClNMR

$ADFBIN/adf -n 4 << eor
Atoms
Au       6.737399000      5.313458000      3.355505000
Cl       8.846057000      6.021952000      3.900499000
P        4.680573000      4.610476000      2.851209000
C        4.658437000      3.608492000      1.343611000
C        5.420052000      4.027537000      0.248711000
C        5.474330000      3.250448000     -0.905963000
C        4.790140000      2.041084000     -0.964047000
C        4.021854000      1.629879000      0.117858000
C        3.950999000      2.409663000      1.269673000
C        3.508585000      5.972710000      2.635244000
C        3.345851000      6.844240000      3.724036000
C        2.451319000      7.907471000      3.639833000
C        1.730236000      8.114115000      2.469827000
C        1.893071000      7.261203000      1.387012000
C        2.776181000      6.181926000      1.466537000
C        3.920170000      3.579461000      4.134266000
C        2.535415000      3.524462000      4.276034000
C        1.968272000      2.680492000      5.229556000
C        2.783661000      1.903281000      6.043519000
C        4.166394000      1.952522000      5.904090000
C        4.740511000      2.791348000      4.948749000
H        5.974510265      4.949617313      0.342219981
H        6.002079605      3.605384243     -1.778832187
H        4.939982538      1.426899001     -1.839674775
H        3.475478388      0.703166299      0.022583344
H        3.336634662      2.090054342      2.098411056
H        3.919676027      6.773206714      4.636219704
H        2.366226939      8.580092235      4.480511307
H        1.101507232      8.988820421      2.392428275
H        1.361960564      7.416872101      0.459602255
H        2.950405194      5.520939498      0.630389420
H        1.918606191      4.035913346      3.551903891
H        0.893161242      2.594711490      5.285934744
H        2.321315210      1.264424433      6.781420522
H        4.818370168      1.385674246      6.552172325
```

```
H        5.805148348      2.848495974      4.776466014
End

relativistic spinorbit zora

symmetry NOSYM

qtens

XC
  lda vwn
  gga becke perdew
end

integration 8

Basis
    Type ZORA/QZ4P
    Core None
End

save TAPE10

End input
eor

$ADFBIN/cpl -n 4 <<eor
nmrcoupling
GAMMA 1 4730600
dso
pso
fc
sd
scf convergence 1e-5
nuclei 1 3
end

ENDINPUT
eor

rm TAPE21 logfile TAPE10
```

A.3. ADF Input file for calculation of J for PMe_3AuCl with a ^{197}Au-^{31}P bond length set to 2.334 Å

```
#!/bin/sh
cd PAuBond

$ADFBIN/adf -n 4 <<eor
Atoms
```

```
Au       0.333141097      0.417675562     -0.324328744
Cl       1.564430594      1.961404438     -1.523047782
P       -0.910941018     -1.142092056      0.886844518
C       -1.891708410     -2.371728909      1.841668340
H       -2.585634137     -1.881219595      2.517238124
H       -2.470107982     -3.010587316      1.181486068
H       -1.247265597     -3.010587316      2.437554368
End

relativistic spinorbit zora

symmetry NOSYM

qtens

XC
  lda vwn
  gga becke perdew
end

integration 8

Basis
  Type ZORA/QZ4P
  Core None
End

save TAPE10

End input
eor

$ADFBIN/cpl -n 4 <<eor
nmrcoupling
GAMMA 1 4730600
dso
pso
fc
sd
scf convergence 1e-5
nuclei 1 3
end
ENDINPUT
eor

rm TAPE21 logfile TAPE10
```